QUANTIFICATION OF IMPURITIES IN PRAIRIE SNOWPACKS AND EVALUATION AND ASSESSMENT OF MEASURING SNOW PARAMETERS FROM MODIS IMAGES

A Thesis

by

JENNIFER NICOLE MORRIS

Submitted to the Office of Graduate Studies of
Texas A&M University
in partial fulfillment of the requirements for the degree of

MASTER OF SCIENCE

August 2011

Major Subject: Geography

Quantification of Impurities in Prairie Snowpacks and Evaluation and Assessment of Measuring Snow Parameters from MODIS Images

QUANTIFICATION OF IMPURITIES IN PRAIRIE SNOWPACKS AND EVALUATION AND ASSESSMENT OF MEASURING SNOW PARAMETERS FROM MODIS IMAGES

A Thesis

by

JENNIFER NICOLE MORRIS

Submitted to the Office of Graduate Studies of
Texas A&M University
in partial fulfillment of the requirements for the degree of

MASTER OF SCIENCE

Approved by:

Chair of Committee,	Andrew G. Klein
Committee Members,	Anthony M. Filippi
	Sorin C. Popescu
Head of Department,	Vatche P. Tchakerian

August 2011

Major Subject: Geography

ABSTRACT

Quantification of Impurities in Prairie Snowpacks and Evaluation and Assessment of Measuring Snow Parameters from MODIS Images. (August 2011)

Jennifer Nicole Morris, B.S., Texas A&M University

Chair of Advisory Committee: Dr. Andrew G. Klein

Extensive research on soot in snow and snow grain size has been carried out in the Polar Regions. However, North American prairie snowpacks lack observations of soot in snow on snow albedo which adds uncertainty to the overall global effect that black carbon on snow has on climate. Measurements in freshly fallen prairie snowpacks in Northwestern Iowa and Central Texas were collected from February 25 to March 3, 2007 and April 6, 2007, respectively.

Multi-day monitoring locations and a frozen lake were study sites at which snow samples were collected to measure soot in snow concentrations. Ancillary measurements were collected at a subset of the sample sites that included: temperature, density, depth, and grain size. At some locations snow reflectance and snow radiance was collected with an Analytical Spectral Device visible/near infra-red spectroradiometer (350 – 1500 nm).

Snow impurity, consisting of light-absorbing particulate matter, was measured by filtering meltwater through a nucleopore 0.4 micrometer filter. Filters were examined using a photometer to measure mass impurity concentration. Soot observations indicate prairie snowpack concentrations ranging from 1 ng C gm^{-1} to 115 ng C gm^{-1} with an

average of 34.9 ng C gm^{-1}. These measurements are within range of previously published values and can lower snow albedo. As expected, spectral albedo was found to decrease with increasing impurities. Additionally, as grain size increased impurity concentration increased. Differences in soot concentration were observed between the two Iowa snowfall events. The Texas event had higher soot concentrations than both Iowa snowfalls.

Validation of an ADEOS-II snow product algorithm that compares simulated radiances to measured sensor radiances for retrieval of snow grain size and mass fraction of soot in snow was attempted using satellite images acquired by the Moderate Resolution Imaging Spectroradiometer (MODIS). The algorithm was unable to uniquely identify a particular snow grain size and soot concentration that would lead to a converging radiance solution in the two spectral bands measured and compared by the algorithm. The *in situ* data at the validation site fell within published ranges for freshly fallen snow for both snow grain size and soot concentration; however; the closest algorithm retrievals were considerably higher than in situ measurements for both grain size and impurity concentrations.

DEDICATION

I dedicate this thesis to my mother, Paula Kay Wilson, for her patience, understanding, and encouragement during this process. This thesis is also dedicated to my sister, Heather Deann Cook, for her limitless moral support and dedication to assisting me in achieving my aspirations. I also dedicate this thesis to the memory of my father, Aury Wayne Morris, who always believed in me. I would not be who I am today if not for my family, and I am extremely grateful for their unconditional love and support.

ACKNOWLEDGEMENTS

After obtaining a bachelor degree from the Department of Geography at Texas A&M University, the thought of pursuing a graduate degree was merely a dream. With the assistance of the Department of Geography and the College of Geosciences, this dream soon became reality. I would like to thank several individuals that brought this dream to fruition. First, I would like to thank the staff and faculty of the Department of Geography. Every request, no matter how small, was catered to and followed through by the many individuals in this department. Their help during this process was crucial to the successful completion of this thesis. I would also like to thank Dr. Vatche Tchakerian, our Interim Department Head, Dr. Jonathon Smith, our Assistant Department Head, and Dr. Dave Cairns, our Graduate Advisor for their continued support and academic advice. I have received help from all of the professors in our department throughout my academic career, but I would like to especially thank Dr. Sarah Bednarz, Dr. Robert Bednarz, Dr. Anthony Filippi, and Dr. Steven Quiring, for their professional advice and encouragement.

I would like to thank my committee chair, Dr. Andrew Klein, for recognizing my potential as a scientist and nurturing my academic ability during my undergraduate and graduate education. His undying patience and time that he puts forth to assure his students success is highly admirable. He provided me with all of the tools and experiences necessary to complete my thesis. His encouragement and persistence during this process has afforded me the opportunity to learn to think independently and assure

that the final product is my own. His focus on my professional development allowed me to meet and collaborate with significant scientists in my field and attend professional conferences. I am forever grateful for his support and continued advice that has greatly increased my perception of myself as a scientist.

I want to acknowledge my other committee members, Dr. Anthony Filippi, and Dr. Sorin Popescu. Dr. Filippi has taught me many lessons important to my professional success outside of the invaluable ideas and concepts taught inside the classroom. His example of work ethic, selflessness, and focus on working as a team to achieve your goals will be carried with me throughout my career. The lessons that he has afforded me have been crucial to my personal success.

I want to thank Dr. Sorin Popescu for always having his door open and showing interest in my project at every turn. His instruction has taught me how to apply theories and concepts learned in the classroom to real world applications. His focus on the importance of professional development will resonate within me for many years to come.

I have received two significant sources of funding to complete my degree, and I would like to acknowledge both of them. First, I thank Dr. Vatche Tchakerian and Roxanna Russell in the Office of the Dean of the College of Geosciences for the graduate assistantship. I would also like to thank Dr. Sarah Bednarz in the Department of Geography for my National Science Foundation Fellowship. These positions provided countless hours of mentoring, support, and dedication to my professional development. The skills and knowledge gained from these positions is invaluable.

The fieldwork associated with this research would not have been possible without the assistance of several people. I would like to thank them all. Dr. Carl Klein and Sharon Klein opened up their home and showed outstanding hospitality throughout the field campaigns associated with this work. Without this home away from home these field campaigns could not have been completed. I would also like to thank Lexi Plumb, Iliyana Dobreva, and Zhaohui Chi for their assistance and interest in completing the field campaigns. The inclement weather in these field campaigns can dull the brightest personalities and their persistence and willingness to learn made the experience truly amazing. I would also like to thank Dr. Andrew Klein for affording me the opportunity to carry out the field work associated with this research. His counsel, advice, and comedic relief made this experience unforgettable. Furthermore, I would like to thank Dr. Stephen G. Warren and Dr. Thomas Grenfell for their interest and guidance throughout this process. They graciously allowed me to visit the University of Washington – Seattle campus to use equipment and techniques that are not otherwise available.

Sincere appreciation and thanks goes to Dr. Teruo Aoki, Dr. Knut Stamnes, Dr. Masahiro Hori, and Dr. Wei Li who exemplify through action the true meaning of scientific progress. These gentlemen originally developed and wrote the ADEOS-II GLI snow product models and algorithms validated in this research. They have cordially provided the code and algorithm for validation purposes for this research. Their dedication to the advancement of this field is highly admirable and volumes could be stated about their drive to produce cutting edge scientific advancements.

Additionally, I would like to thank the graduate student body in the Department of Geography at Texas A&M University. Without hesitation, students have stopped progress on their own work to help me find solutions or creative ideas that assisted in this research. I would like to especially thank Joni Kincaid, Nikki Williams, Adriana Martinez, and Stephen Berhane for countless hours of advice, trouble shooting, and willing me to move forward at times when all hope seemed lost.

Last but not least, this process would have led to insanity without the support, care, guidance, and patience of all of my loved ones, friends, and family. I would specifically like to thank Elliott Templeton, Stephanie Grounds, Justin Stachnik, Heather Vansciver, and Diane McLendon for keeping me sane throughout this process. Friends and loved ones are truly the individuals who carry you when you have forgotten how to fly. Thank you for reminding me how to soar. The gratitude and appreciation that I owe to my family could fill volumes, and I therefore must simply say thank you. All of the aforementioned individuals, and so many more, have brought my dream to fruition and I thank you all for impacting my life in such a positive fashion that will resonate with me throughout my professional career.

NOMENCLATURE

AGL	Above Ground Level
ARL	Air Resources Laboratory
ASD	Analytical Spectral Devices
BC	Black Carbon
C	Carbon
cm	centimeter
CO	Carbon Monoxide
EPA	Environmental Protection Agency
ft	feet
GLI	Global Imager
gm	gram
HYSPLIT	Hybrid Single-Particle Lagrangian Integrated Trajectory
IDL	Interactive Data Language
IP	Integrating Plate
IP-NDF	Integrating Plate with Neutral Density Filter
IPCC	International Panel on Climate Change
IR	Infra-red
IS	Integrating Sphere
ISSW	Integrating Sandwich that incorporates an Integrating Sphere
ISW	Integrating Sandwich

km	kilometer
LUT	Lookup Table
m	meter
μm	micrometer
mi	mile
ml	milliliter
mm	millimeter
NIR	Near Infra-red
nm	nanometer
NCEP	National Center for Environmental Protection
NOAA	National Oceanic Atmospheric Administration
NOx	Nitrogen Oxides
NWS	National Weather Service
MODIS	Moderate Resolution Imaging Spectroradiometer
O3	Ozone
PM	Particulate Matter
PM-2.5	Particles less than 2.5 microns
PM-10	Particles less than 10 microns
ppbw	Parts per billion weight
ppmw	Parts per million weight
r	Radius
RF	Radiative Forcing

SO2	Sulfur Dioxide (SO2)
TOA	Top of Atmosphere
VOC	Volatile Organic Compounds
W	Watt

TABLE OF CONTENTS

Page

LIST OF FIGURES

FIGURE Page

LIST OF TABLES

1. INTRODUCTION

The presence of impurities in snow can significantly decrease snow albedo and affect snowmelt. Impurities in snow and ice have recently been acknowledged as one of the largest uncertainties in estimates of global radiative forcing (RF) due to an insufficient understanding of snow impurity concentrations, specifically black carbon effect on snow. The best estimate for the RF of black carbon (BC) on snow is +0.10 ± 0.10 W m^{-2}, but the scientific level of certainty is low (Forster et al., 2007). Furthermore, Northern Hemisphere land areas yield an estimated BC influence on snow RF of +0.3 W m^{-2} (Hansen and Nazarenko, 2004). It is important to note that the combined global RF for anthropogenic sources is estimated at +1.6 $[-1.0, +0.8]^2$ W m^{-2} (Forster et al., 2007). Due to this insufficient understanding of impurities and their radiative effects, it is essential to further examine fundamental gaps in the current scientific body of knowledge by completing additional studies.

Previously published measurements in conjunction with radiative transfer modeling indicate that parts-per-billion amounts of snow impurities can decrease snow albedo considerably (Wiscombe and Warren, 1980) and potentially affects prairie snowpacks. Snow grain size also plays an important role in determining the relationship between the spectral albedo of snow and mass impurities because as grain size increases spectral albedo decreases at all wavelengths (Warren, 1984; Wiscombe and Warren, 1980).

This thesis follows the style of *Remote Sensing of Environment*.

As snow ages, grain size generally increases due to metamorphism reducing albedo. More importantly, this effect will be amplified if the grain size increases as a function of depth (Warren, 1982). The relationship between and among spectral albedo, snow impurities, and grain size must be further examined to increase scientific certainty of the impact of impurities on snow albedo and snow melt.

1.1 Objectives of the Research

The objectives of this research are to: (1) quantify mass impurities and spectral albedo in recently-fallen snow over several snow events in Spirit Lake, Iowa and Belton, Texas and compare the measured mass impurities concentration and spectral albedo to published information for Polar Regions and industrialized areas, (2) evaluate and compare three snow events for temporal and regional differences in relation to impurity concentration and snow grain size, and (3) validate ADEOS-II/GLI snow products that include snow extent, two estimates of snow grain size, and mass concentration of snow impurities using Moderate Resolution Imaging Spectroradiometer (MODIS) images of Spirit Lake, Iowa and compare the ADEOS-II algorithm retrievals of soot and grain size to *in situ* measurements.

This research fills in three significant gaps within the climate change and cryosphere domains. It will help increase scientific certainty on the effects of black carbon as a RF in global climate change. The International Panel on Climate Change (IPCC) reports that a low level of scientific certainty on the effects of black carbon as a RF is partially due to the lack of *in situ* surface albedo measurements (Forster et al., 2007). The *in situ* albedo measurements collected for objective one of this study can be

combined with other studies to more accurately estimate the BC on snow RF. Secondly, previous research conducted examining snow impurities and its effect on snow albedo is limited to mountainous areas (Grenfell et al. 1981), the Arctic (Clarke and Noone, 1985; Grenfell et al., 2002), Antarctic (Grenfell et al., 1994; Warren and Clarke, 1990), China (Huang et al., 2011) and Japan (Aoki et al., 2000).

The focus of objective one will be the first study of its kind to evaluate the relationship between spectral albedo and mass impurities in the prairie snowpacks of the North American Great Plains. An array of snow algorithms and models have been developed to estimate albedo (Dunkle and Bevans, 1956; Giddings and LaChapelle, 1961; Barkstrom, 1972; Barkstrom and Querfeld, 1975; Bohren and Barkstrom, 1974; Berger, 1979; Choudhury and Chang, 1979a, b; Choudhury and Chang, 1981; Wiscombe and Warren, 1980), impurities (Aoki et al., 2000; Stamnes, 1999a, b: Tanikawa et al., 2001), and grain size (Aoki et al., 2000; Li et al., 2001; Stamnes, 1999a, b; Stamnes, 2003; Tanikawa et al., 2001). However, these models have not been widely validated. This lack of validation is primarily the result of the limited amount of *in situ* measurements collected for snow albedo, grain size, and impurities. By validating the current ADEOS-II/GLI snow products in objective two, this cryospheric model can be utilized in future research with significant confidence in the model output. ADEOS-II/GLI snow products encompass two estimates of snow grain sizes and mass concentration of snow impurities, snow surface temperature, and snow/sea-ice cover extent (Stamnes, 1999a). This research will not focus on the latter two, but will utilize collected *in situ* measurements to validate snow grain size and mass concentration of

snow impurities. Model validation is an important role in the scientific process and must be completed if these models are going to be used as the theoretical basis in cryospheric studies.

2. BACKGROUND

2.1 Modeling the Spectral Albedo of Snow

The presence of dark particles in snow causes accelerated snowmelt and lowers snow albedo. Warren and Wiscombe established through radiative transfer modeling that diminutive amounts of impurity in a snowpack can have a significant effect on snow albedo as shown in Figure 1 (Figure 8b of Warren and Wiscombe, 1980). Their ground breaking studies found that in the visible and ultra-violet wavelengths the computed albedo of snow is independent of grain size. Across a range of grain radii (r = 50 – 1000), the snow albedo approached 1.0 for all cases less than 700 nm (Wiscombe and Warren, 1980). At near-infrared (NIR) wavelengths, the computed albedo of snow was sensitive to grain size and decreased as the grain radii increased for all wavelengths greater than 700 nm; this is due in part to ice having strong absorption at near-infrared wavelengths (Wiscombe and Warren, 1980). Additionally, the albedo is lower across all wavelengths for coarse-grained snow due to the consecutive refraction of the re-emerging light through several snow grains; only partially contributing to this effect is external reflection at the top surface of the snow pack (Bohen and Barkstrom, 1974).

The results from Wiscombe and Warren's study are shown in Fig. 2 where they illustrated the model-calculated albedo of snow as a function of wavelength for five different grain radii (Figure 8a of Wiscombe and Warren, 1980). Wiscombe and Warren's results established that impurities in a snowpack are more accurately measured

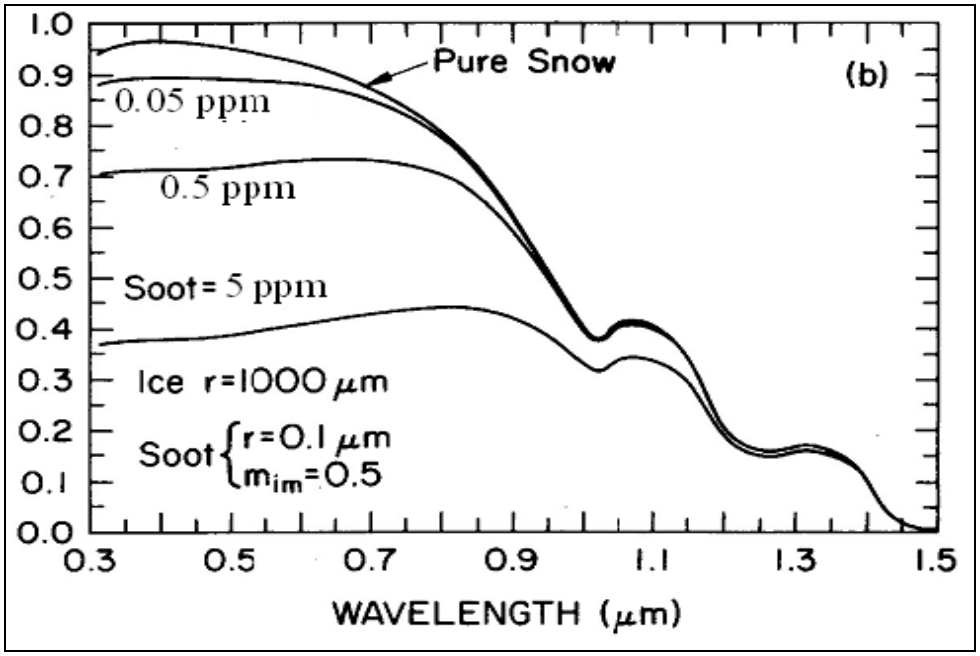

Fig. 1. Effect of soot concentrations on spectral albedo of snow (Warren and Wiscombe, 1980).

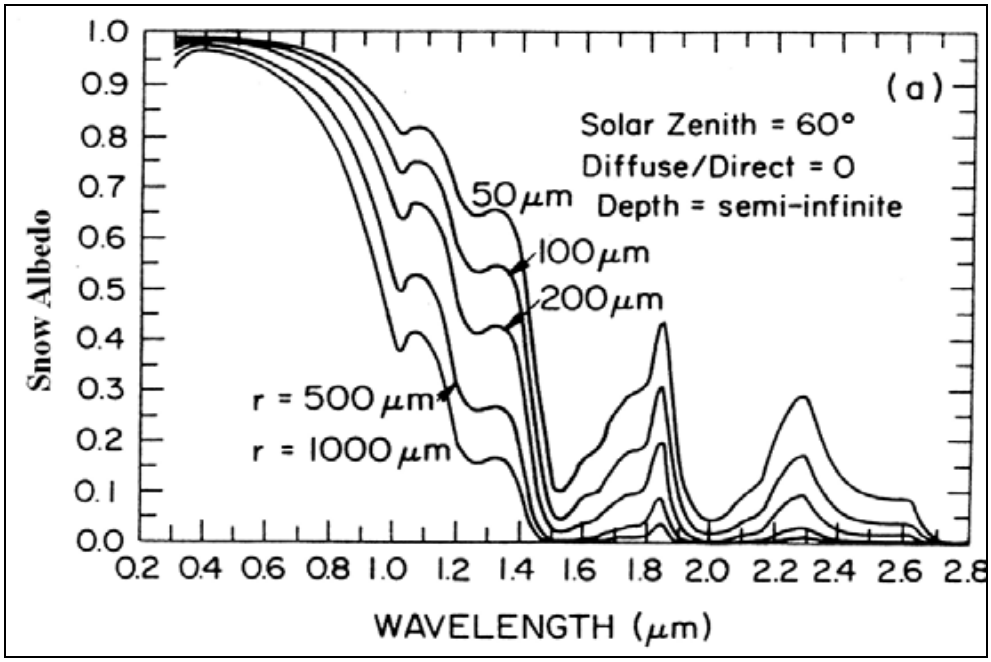

Fig. 2. Model-calculated albedo of snow as a function of wavelength for five different grain radii (Wiscombe and Warren, 1980).

at visible wavelengths than at near-infrared wavelengths due to the near-infrared dependency on grain size (Wiscombe and Warren, 1980).

These results established two important criteria for this study. First, photometric analysis in this research must concentrate on the visible portion of the electromagnetic spectrum where the results will not be affected by grain size. Second, this study must focus on freshly fallen snowpacks where the effect of higher absorption on coarse-grained snow is mitigated as there has been less time for snow metamorphism to occur.

2.2 Impurities in Snow

Impurities in snow that cause considerable absorption of light are dust or soil sediment, volcanic ash, and black carbon or soot. Snow is a highly reflective surface and therefore the presence of black carbon (BC) and dust particles can significantly reduce albedo (Warren, 1982). From these particulate sources, the most effective impurity per unit mass is black carbon; at visible wavelengths 10 nanograms of black carbon per gram of snow have been shown to reduce snow albedo by 1% (Figure 2 of Warren and Wiscombe, 1985). Black carbon particles are produced by incomplete combustion in coal burning, wood or forest fires, and diesel engines (Bond et al., 2004). Black carbon is approximately 50 to 200 times more effective at absorbing sunlight than soil dust or volcanic ash, respectively (Wiscombe and Warren, 1980).

Black carbon in snow has been identified as one of the largest sources for uncertainty when assessing radiative forcings for climate change (Hansen et al., 2005). Soil dust also plays a role in accurate impurity concentrations. Soil sediment and dust is generally visible to the naked eye and appears brown or red in nature whereas BC is

generally colorless and does not appear dirty to the naked eye. Soil dust is a less effective absorber of light than BC but cannot be disregarded in this research.

Impurity concentration is also dependent on grain size as there is an increase in absorption and a significant reduction in albedo in coarse-grained snow. Light penetrates deeper in coarse-grained snowpacks due to the longer distance the light must travel through each snow grain. This extended light exposure in coarse grains results in a higher absorption which results in lower albedo. Furthermore, this dependency on grain size is accentuated by the natural process of snow metamorphism by which snow grains merge causing an increase in grain size and space which further effects the impurity concentration in older snow.

Black carbon measurement has been limited to mountainous areas (Grenfell et al., 1981), the Arctic (Clarke and Noone, 1985; Grenfell et al., 2002; Doherty et al., 2010), Antarctic (Grenfell et al., 1994; Warren and Clarke, 1990), China (Huang et al., 2011) and Japan (Aoki et al., 2000), but until this study there have not been observations of BC over North American prairie snowpacks. Therefore this research focuses on the visible portion of the electromagnetic spectrum where snow models indicate that spectral albedo is relatively insensitive to grain size and the expected decrease in spectral albedo due to increasing contaminants can be most correctly quantified in freshly fallen North American prairie snowpacks.

2.3 Snow Collection and Filtration

Previous studies all use snow collection and filtration methods, or derivatives thereof, developed by Clarke and Noone (1985) where snow samples are collected in glass jars, kept frozen till the time of filtration, melted in a microwave oven, and passed through a nucleopore filter with the use of a partial vacuum. An advantage of this technique is the ability to remotely filter snow at temporary laboratory facilities and thereby eliminate the need to transport high quantities of frozen snow samples to a permanent laboratory setting. This method also accounts for frozen snow to be quickly melted and for particulate extraction to occur immediately (< 1 minute). Following this protocol diminishes the effects of chemical reaction or algae growth after sampling (Clarke and Noone, 1985). This research utilized the sampling and filtration methods described by Clarke and Noone (1985).

2.4 Photometric Analysis

Techniques studied and used in this research are optical. Five prominent optical techniques have been addressed in the literature. These techniques include: (1) integrating plate (IP), (2) integrating plate with neutral density filter (IP-NDF), (3) integrating sandwich (ISW), (4) integrating sphere (IS), and (5) integrating sandwich that incorporates an integrating sphere (ISSW).

The IP method is simplistic in design and therefore widely used in investigations. The IP method consist of a light diffusing support to provide a Lambertian light source on which the filter can be placed (Clark et al., 1987). The IP method shortcoming has been a systematic overestimation of the absorption of light by fine particles. This

launched the creation of the IP-NDF method to reduce this form of bias. The IP-NDF simply placed a neutral density filter between the Lambertian reflector and the sampling filter (Clarke et al., 1987). In the ISW method the substrate, or sample filter, is placed between two diffuse reflectors with a diffuse reflectance of approximately 96% (Clarke et al., 1987). This method was developed for low impurity concentrations. These techniques are non destructive to the substrate or sample filter.

As described in Clarke et al. (1987), the IS technique is a destructive sample method in which a sphere is illuminated through a small hole. The sample is suspended in the center of the sphere where the source light illuminates it. The reflected light is partially absorbed and partially transmitted by the filter or reflected onto the sphere walls. The reflected light is then measured through another hole in the sphere. When using this technique the test filter is dissolved and suspended in a solution placed in a glass flask (Clark et al., 1987). The advantages and disadvantages associated with these techniques are presented elsewhere (Clarke et al., 1987; Lin et al., 1973; Clarke, 1982a; Clarke 1982b).

The technique utilized in this study is the most recent form of these techniques. The ISSW technique (Grenfell et al., 2011) is a non destructive substrate method that combines an integrating sphere and an integrating sandwich approach in which an integrating sandwich spectrophotometer incorporates an integrating sphere as one side of the sandwich (Doherty et al., 2010). The use of this technique is further described in the filter photometric analysis section of the methods section.

2.5 Trajectory Modeling

The National Oceanic and Atmospheric Administration (NOAA) and Air Resources Laboratory (ARL) developed a first of its kind web-based atmospheric modeling suite that can display meteorological data and atmospheric transport model products that were previously only available to ARL scientists. ARL joined efforts with the National Center for Environmental Protection (NCEP) of the National Weather Service (NWS) in order to gain access to meteorological observations and forecast model fields for use in atmospheric dispersion models such as the Hybrid Single-Particle Lagrangian Integrated Trajectory model (NOAA ARL HYSPLIT model) (Draxler and Rolph, 2003). The HYSPLIT model is ARL's transport and dispersion model. This model allows users to produce air parcel trajectories that follow the movement of the wind patterns defined by the meteorological models run operationally by the NOAA NCEP as well as archived meteorological observations. Meteorological data in both forecast and archive formats are available to HYSPLIT on global and regional scale grids. This web-based model allows access to tools that provide the user with quick access to meteorological data that can be used to model from a specific location of interest. In this research, the HYSPLIT model was utilized in conjunction with archive NWS data to model the backwards trajectory of the air parcels associated with the snowfall events that occurred throughout the field campaign.

2.6 ADEOS-II GLI Snow Products

The ADEOS-II GLI snow product codes CTSK1ab and CTSK2b1 are broken down into three separate codes that can perform cloudy/clear discrimination (CTSK1a),

snow/sea-ice discrimination (CTSK1b), and retrieval of snow grain size and mass fraction of soot mixed in the snow (CTSK2b1) (Stamnes, 1999a, b). This research focuses on the retrieval of snow grain size and mass fraction of impurities mixed in the snow. This algorithm is based on the grain size dependency of the reflectance of snow in the near infra-red (NIR) and pollution in the visible portion of the electromagnetic spectrum (Stamnes, 1999a). This algorithm can be applied to both high- and mid-latitude regions under clear sky conditions.

The retrieval procedures of snow properties for ADEOS-II/GLI are as follows. In order to relate physical attributes such as grain size to snow reflectance the algorithm utilizes a radiative transfer model to produce a set of lookup tables (LUTs). These LUTs are based on simulated radiances for GLI (Global Imager) channels 5 (0.46 μm), 19 (0.865 μm), and 28 (1.64 μm) (Stamnes et al., 2007). Based on the theoretical foundation provided by Warren and Wiscombe, Figure 3 (Stamnes et al., 2007) shows that in the visible portion of the electromagnetic spectrum the ADEOS-II/GLI model is less dependent on grain size (GLI 5) than in the near infrared (GLI 19). The Simulated radiances are calculated as a function of snow grain size (50 – 2000 μm) and the mass fraction of soot (0.02 to 2.5 ppmw) (Stamnes et al., 2007). The range for snow grain size is suitable because the average grain size found in nature is 40 – 100 μm for new snow, 100 – 300 μm for fine-grained aged snow, and 1000 – 1500 μm for aged snow close to the melting point (Wiscombe and Warren, 1980). In addition, radiance, solar zenith angle, sensor viewing angle, and relative azimuth angle are also taken into account when creating the LUTs. The retrieval of the snow properties is then carried out by finding the

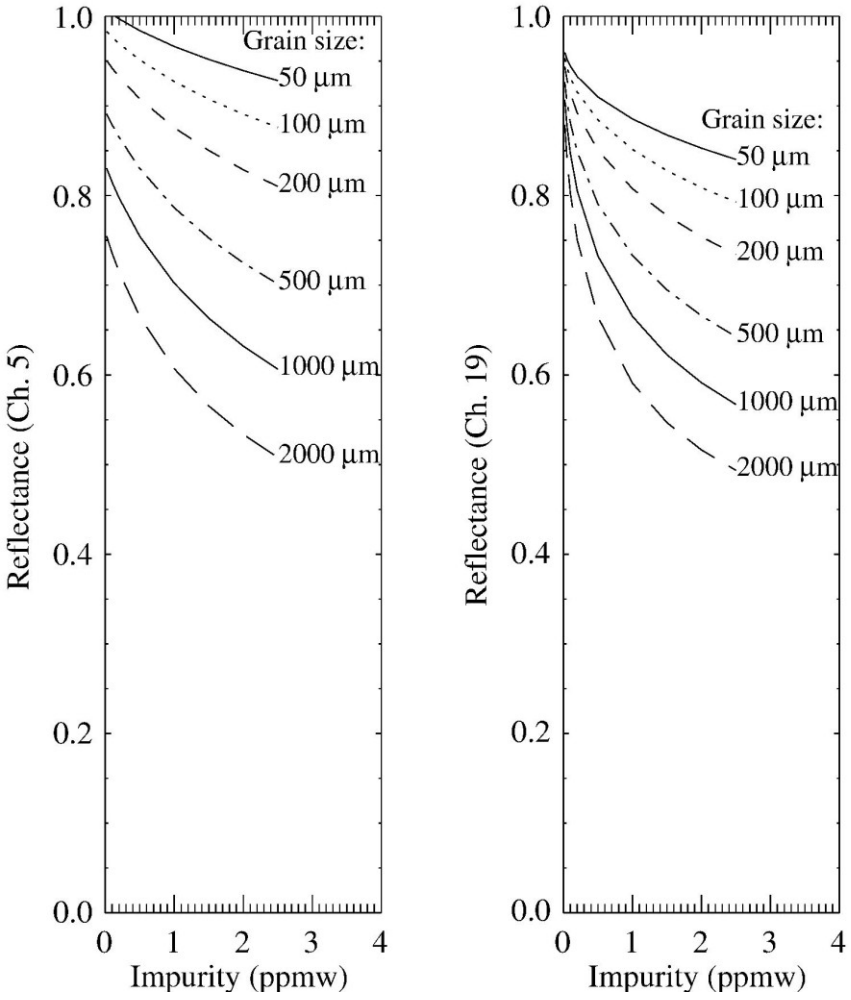

Fig. 3. GLI algorithm estimated snow parameters as a function of reflectance (Aoki et al., 2000).

best match between the measured satellite radiance for an individual pixel being analyzed in the image with a specific entry in the LUT (Stamnes et al., 2007). Therefore, the final results are acquired when the simulated radiances correspond to measured radiances. This retrieval procedure is utilized for clear-sky conditions and snow-covered pixels.

3. STUDY AREA AND SAMPLING STRATEGY

3.1 Study Area Overview

The first study area for this research is located in Dickinson County surrounding the county seat of Spirit Lake and the town of Okoboji (Fig. 4). Dickinson County is located in northwest Iowa along the Minnesota border and is home to the Iowa Great Lakes. According to the United States Census Bureau, Dickinson County has a total area of 1,046 km^2 (404 mi^2). Approximately 987 km^2 (381 mi^2) of which is land and 59 km^2 (23 mi^2) is water (United States Census Bureau, 2010). Most of Dickinson County is under cultivation typical of the Midwestern United States. This area comprises a flat topography with very sparse forest cover, and therefore, is used primarily for agricultural farmland. The 2010 United States Census reported the population of Dickinson County as 16,667 with a population density of 15.93 people per square mile (United States Census Bureau, 2010).

3.1.1 Dickinson County Emissions Summary

Industrialized countries and remote regions need be concerned with the deleterious effects that anthropogenic emissions of acidic pollutants are posing on their ecosystems. This concern has moved to the forefront of seasonal snow cover studies in recent years as seasonal snow cover is a key factor in the transport of atmospheric pollutants (Davis et al., 1987). All data for this emissions summary was provided by the Environmental Protection Agency Air Data Reports and Maps and is summarized below:

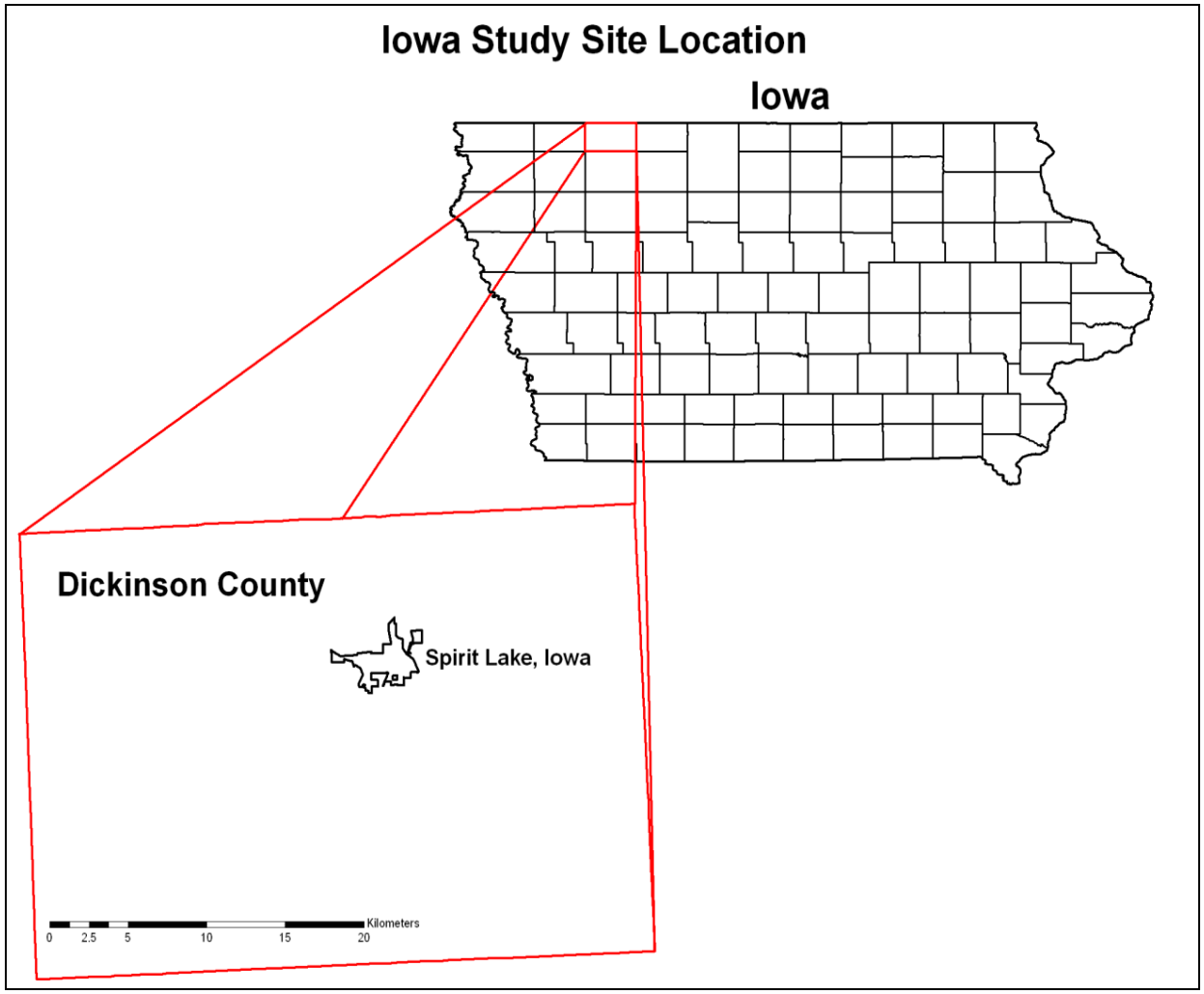

Fig. 4. Dickinson County, Iowa study site location.

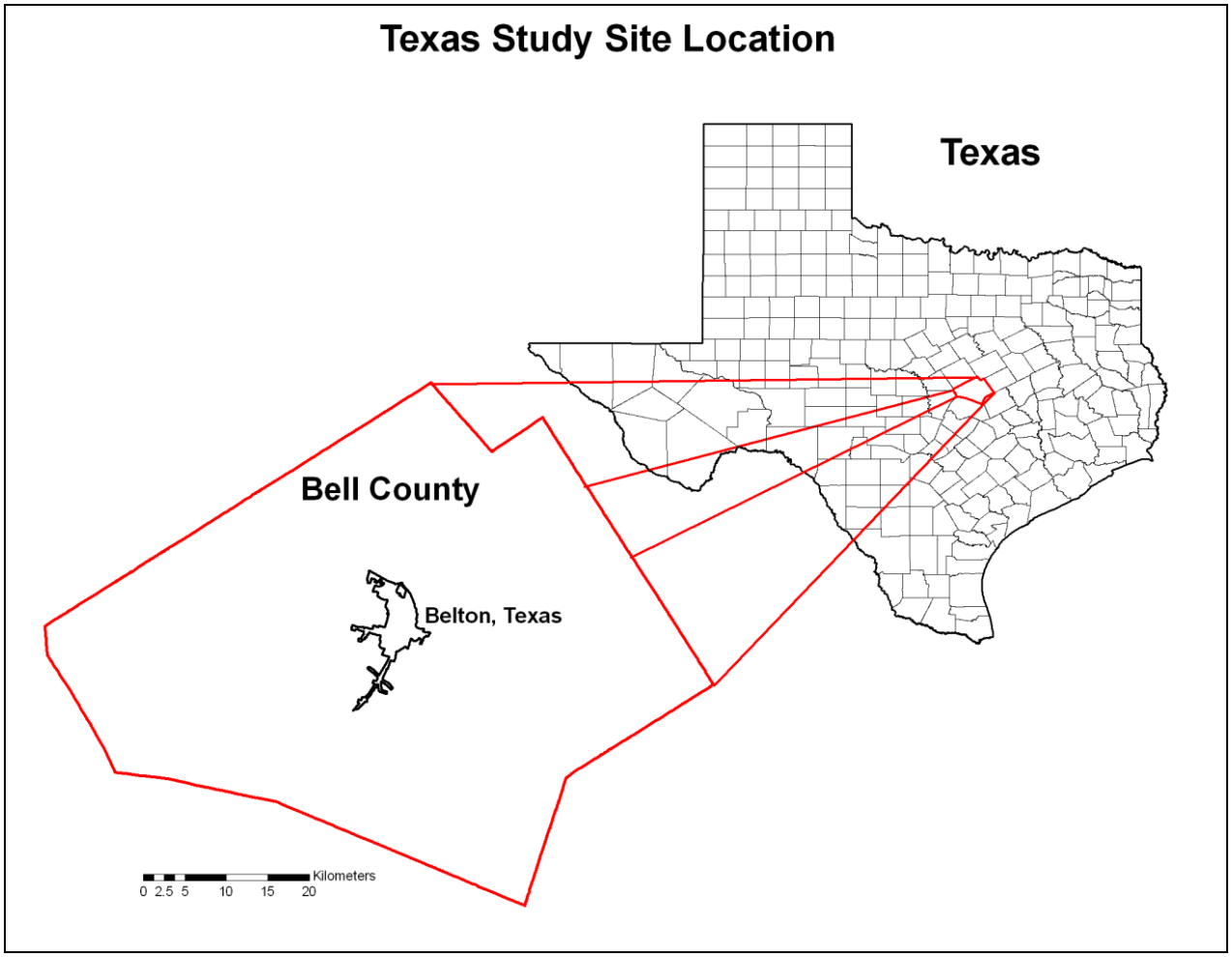

Fig. 5. Bell County, Texas study site location.

> In terms of anthropogenic smog and particulate matter, carbon monoxide (CO), nitrogen oxides (NOx), PM-2.5 (particles less than 2.5 microns), PM-10 (particles less than 10 microns), sulfur dioxide (SO2), and volatile organic compounds (VOC) emissions are all present in the Dickinson County environment. The two major emissions sources are transportation vehicles and stationary combustion sources such as electric utility and industrial boilers. Particulate matter includes dust, dirt, soot, smoke and liquid droplets directly emitted into the air by sources such as factories, power plants, cars, construction activity, fires and natural windblown dust (Environmental Protection Agency, 2011).

When examining Dickinson County on a zero to one hundred percentile scale, where 0% equals the cleanest/best counties in the United States and 100% equals the dirtiest/worst counties in the United States, Dickinson County, Iowa ranks in the 20th percentile in PM-2.5 and in the 30th percentile in PM-10. The EPA 1999 Emissions Summary showed that 56.20% (521 T) percent of PM-2.5 pollutants emitted comes from area sources while the remaining 43.80% (406 T) were from mobile sources. 55.33% (2,376 T) of PM-10 emissions were attributed to area sources while 44.67% (1,918 T) were deemed mobile sources (Environmental Protection Agency, 2011).

The second study area is located in Bell County, Texas with sample sites located in the county seat of Belton (Fig 5). Bell County is located in central Texas and has a total area of 2,818 km^2 (1,088 mi^2) according to the United States Census Bureau. The

county is comprised of 2,745.4 km^2 (1,060 mi^2) of land and 72.5 km^2 (28 mi^2) of water (United States Census Bureau, 2010). Similar to the Iowa study site, this area consists of a flat topography with little to no forest cover and is also used primarily for agricultural farmland. The 2010 United States Census reported the population of Bell County as 310,235 with a population density of 292.7 people per square mile (United States Census Bureau, 2010).

3.1.2 Bell County Emissions Summary

The EPA 1999 Emissions Summary for Bell County, Texas reported staggering results for particulate matter emissions. Bell County ranks in the 90th percentile for both PM-2.5 and PM-10 emissions falling in line with the dirtiest or worst counties in the United States. The report attributes the particulate matter emissions to mobile, area, and point sources for a combined 4,964 tons of pollutant emitted. Mobile sources made up 75.06% of PM-2.5 emitted, while 23.41% and 1.51% were assigned to area and point sources, respectively. For PM-10, 26, 277 tons of pollutants were reported by the EPA with mobile, area, and point sources comprising 77.23%, 20.50%, and 0.36%, respectively (Environmental Protection Agency, 2011).

The land use/land cover attributes of Dickinson and Bell County coupled with the lack of observations in North American prairie snowpacks make the locations ideal sites for snow impurity research. Additionally, Big Spirit Lake offers an ideal validation site for satellites with relatively large pixel sizes, such as the 250 to 500 meter pixels of MODIS due to the limited traffic on the lake and sparse forest cover around the lake.

3.2 Sample Sites Overview

Two different types of sampling sites were utilized in the Dickinson County study area. These sites are comprised of a natural lake and twelve multi-day monitoring sites. A frozen natural lake was selected as a sample site due to its flat uniform surface that has little or no human impact on the snowpack. This frozen lake site was used to validate ADEOS-II\GLI snow products. In addition, twelve selected multi-day monitoring sites were monitored for mass impurity concentration over the course of the field campaign making it possible to examine spatial and temporal differences between new and old snow as well as differences between snow fall events.

The Central Texas field campaign also consisted of twelve sample sites. These sites are all presumed to have low human impacts on snow impurity measurements due to the short time and nature of the snow fall event studied.

3.3 Sample Site Locations

The first study site is located on Big Spirit Lake (Fig. 6). Big Spirit is a natural lake spanning over 2,300 ha (5,684 ac) with 25.54 km (15.25 mi) of shoreline and is the largest lake in Iowa (United States Census Bureau, 2010). It is one of the lakes that comprise the chain of lakes known as the Iowa Great Lakes. The northern shore of this lake straddles the borders of Iowa and Minnesota. The maximum depth of Big Spirit Lake is 7.3 m (24 ft) with a mean depth of 5 m (17 ft) (United States Census Bureau, 2010). In geomorphic terms, Big Spirit Lake is a glacial pothole or kettle hole and is a remnant of the most recent ice age approximately 13,000 years ago. Kettle holes are characterized by sediment-filled water bodies that are usually shallow in nature and

formed by retreating glaciers or draining floodwaters. This site was selected due to its size and limited human impact on the snowpack covering the frozen lake. Furthermore, Big Spirit Lake was selected as the main validation site for MODIS as it is larger than 500 x 500 meters, the spatial resolution of one MODIS pixel. The 500 x 500 meter validation site was broken down into a 16 sub grids, where each grid block comprises a 125 x 125 m area with one sample site randomly selected within each grid block (Fig. 7).

The multi-day monitoring locations were sampled in the town of Spirit Lake, Iowa. The total land area of Spirit Lake is 8.62 km^2 (3.33 mi^2) with a population density of 1387 people per square mile (United States Census Bureau, 2010). Within Spirit Lake, 12 sampling sites were selected to monitor and revisit over the course of the field campaign (Fig. 8). By establishing monitoring sites and resampling these locations, determining the changes in impurity concentration over the course of two snowfall events was achieved.

Twelve selected sites in Bell County were sampled in the town of Belton, Texas (Fig. 9). The total land area of Belton is 34.1 km^2 (13.2 mi^2) with a population density of 1,171 people per square mile (United States Census Bureau, 2010). Snowfall events in this region are unique and often unforeseen; therefore it was important to collect these samples as quickly as possible due to the rapid snowmelt of this snowpack. To facilitate comparison with the previous Iowa field campaign, 12 sites that were spatially dispersed across the town of Belton were selected.

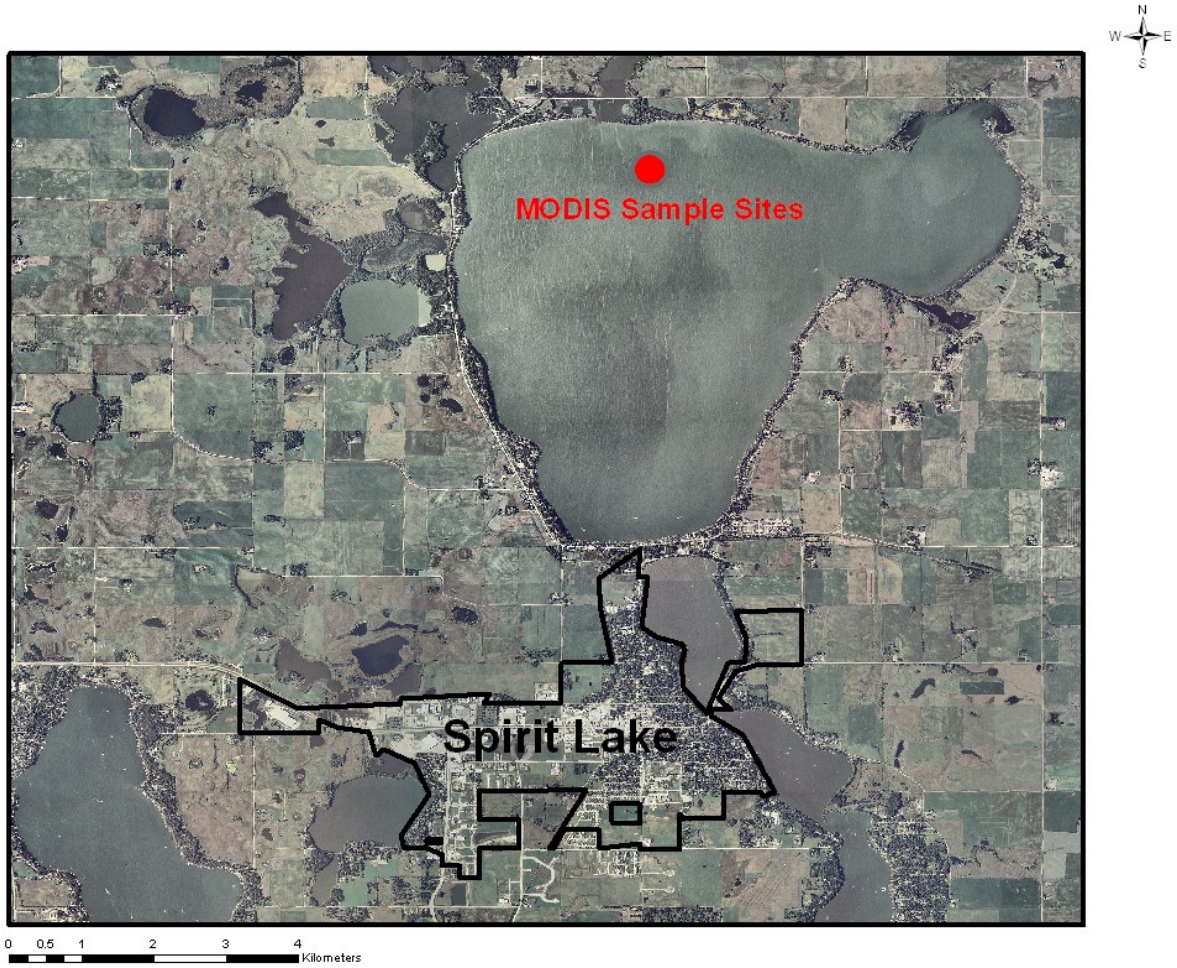

Fig. 6. MODIS sample site location.

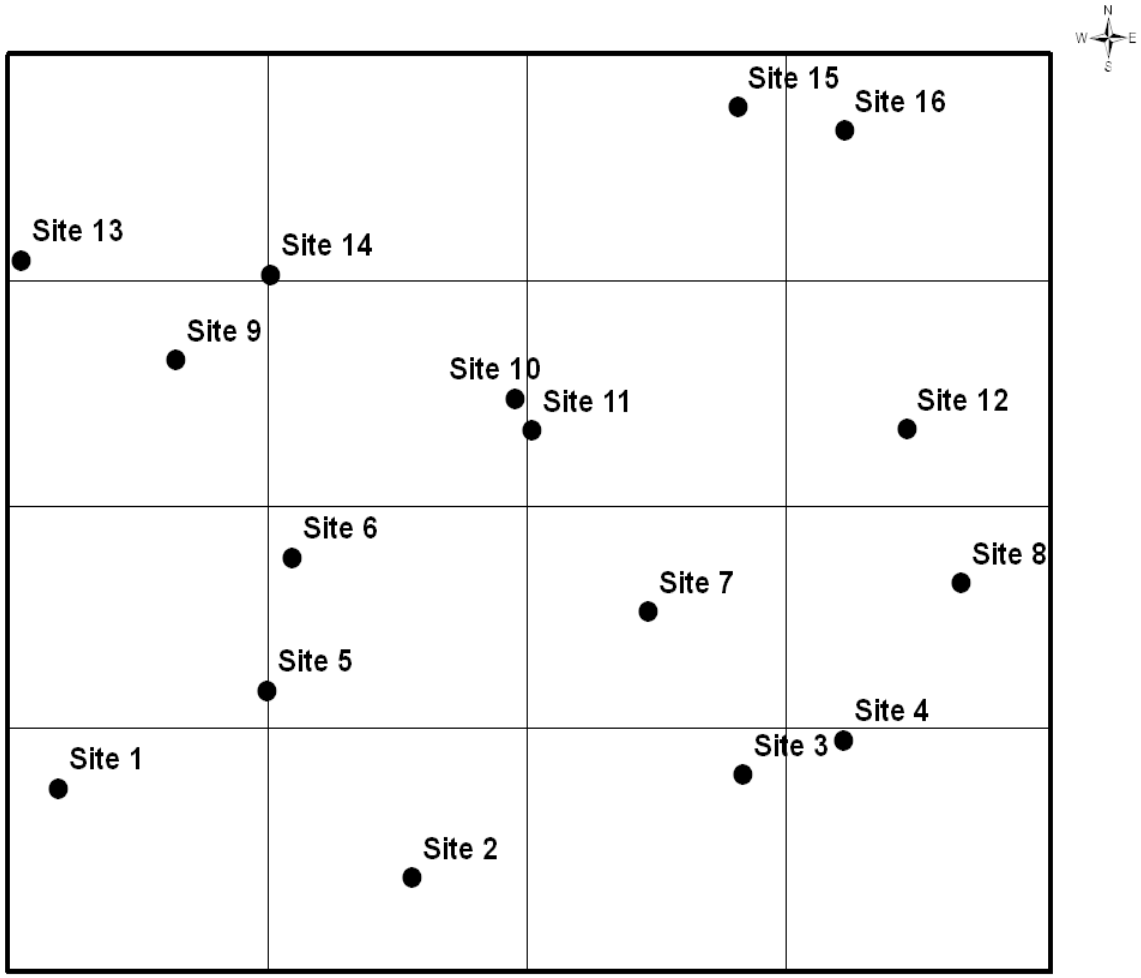

Fig. 7. MODIS sample site grid.

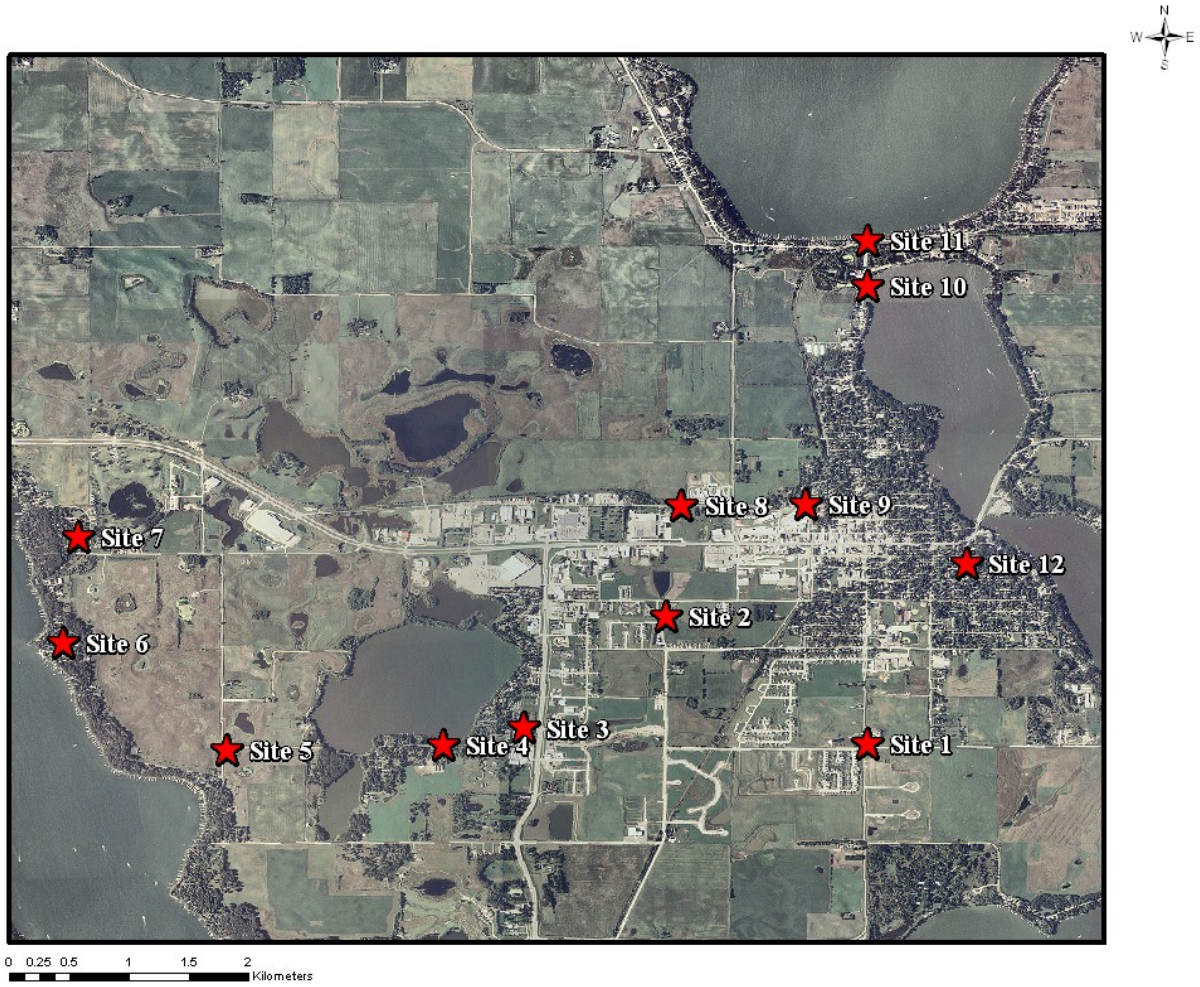

Fig. 8. Spirit Lake, Iowa site locations.

Fig. 9. Belton, Texas site locations.

3.4 Snow Sampling Events

From February 25th to March 2nd, 2007, twelve multi-day monitoring sites in Dickinson County, Northwestern Iowa were each sampled three times to examine the particulate loading in the snowpack. These samplings are identified as Sampling 1, Sampling 2 and Sampling 3. The sites were a selected representation of the regions physical and built landscape that could be safely accessed following a major snowstorm. Sampling 1 is representative of a freshly fallen snowpack from a storm front that reached the site on February 25, 2007 and continued into February 26, 2007. This storm system deposited 20.3 cm of snow of the course of two days. Sampling 2 occurred 24 hours following the original sampling. Sampling 3 represents a second snow storm that occurred on March 2, 2007 and deposited 33 cm of new snow on top of the existing snowpack.

In addition to these events, a rare Central Texas snow storm that occurred on April 6, 2007 and resulting in 8.6 cm of snowfall represents a unique opportunity to examine particulate loading in the fresh snowpack in the southern United States and is represented here as Sampling 4.

The locations of these events are unique for snow impurity studies. As previously stated, an overwhelming amount of research has taken place in the Polar Regions on snow impurities and its effects on snow albedo. This study is the first of its kind to analyze the effects of snow impurities on northern hemisphere mid-latitude snowpacks. Additionally, the Central Texas event is specifically extraordinary due to the infrequent snowfall in this region.

3.5 Sampling Strategy

The Northwestern Iowa multi-day monitoring sites were dispersed throughout Dickinson County (Fig. 8) to create a spatial sampling distribution that included both residential and rural sites. These sites were then qualitatively rated based on presumed level of human impact as “low”, “medium”, and “high”, with low sites considered to have the least human impact effect on snow impurity measurement and high sites comprising the strongest effect. This sampling strategy assures a comprehensive representation of North American prairie snowpacks at defined levels of human impact with both residential and rural depiction for a temporal analysis of impurities in snow.

The Central Texas sites (Fig. 9) were selected to include both residential and rural locations in the sampling distribution. These sites are all presumed to have a “low” human impact effect on snow impurity measurements due to the time and nature of this event. Sites in Central Texas were sampled once due to the rapid melting of this snowpack.

This sample strategy made it possible to examine spatial and temporal differences between freshly fallen and time-elapsed snowpacks as well as any differences that may exist between snow fall events.

4. METHODS

4.1 Snow Sampling and Filtration Techniques

Standard techniques for the measurement of black carbon in snow have been developed by Warren, Grenfell, and Clarke and have been widely used in Polar Region studies (Warren and Clarke, 1990; Grenfell et al., 1994, 2002; Warren et al. 2002, Doherty et al., 2010). These techniques are utilized in this study. The measurement technique employed is optical due to the focus on albedo which is a measurement that provides the radiative properties of impurities. Since importance is placed on determining the absorption accurately, the simple filter-transmission methods utilized in the previous Polar Region studies and described below is followed.

To collect samples suitable for this analysis, snow was collected in 500 ml glass jars precleaned to meet Environmental Protection Agency (EPA) Protocol A Level 1 standards for contaminants. Samples were obtained by placing the opening of the glass jar perpendicular to the horizontal surface of the snowpack and pressing the jar through the snowpack until the snow completely filled the jar. Care was taken so the surface was only sampled once. Snow was then removed parallel to the jar enabling a metal spatula to be placed underneath the jar to prevent loss of snow during removal.

Samples were kept frozen until filtration. Freezing was necessary as the particulate can adhere to the glass wall of the jar if the snow melts (Ogren et al., 1983). Therefore it is important to minimize the time that meltwater is in contact with the jar. Furthermore, once the snow is melted, biological activity may develop in the meltwater

and lead to additional absorption or chemical reaction after sampling. To prevent these issues, snow was quickly melted in a microwave oven (less than 2 minutes) and immediately filtered (average of 3 to 5 minutes) through a 0.4 micrometer nucleopore filter using an aspirator to create a partial vacuum. Filtration can cause particle loss to the filtration system using this technique. This particulate loss was reported by Clarke and Noone to be of the order of 10% (Clarke and Noone, 1985). In addition to particulate loss to the filtration vessel, previous studies also show that approximately 15% of the particulate matter can pass through a 0.4 micrometer nucleopore filter (Clarke and Noone, 1985; Doherty et al. 2010). The filters were then placed in covered plastic Petri dishes and air-dried to preserve the sample.

4.2 Sample Standard Measurements

An initial estimate of mass impurity concentration was performed on the dry samples by comparing filters to a set of filter reference standards that provide a close approximation of the mass impurity concentration. These reference standards, produced by Stephen Warren and Thomas Grenfell at the University of Washington, are made combining filtered water, isoprophyl alcohol and India ink; the color of the reference standard is associated with an approximate mg BC cm^{-2} of the filter. The mg BC cm^{-2} are then multiplied by the area of the 0.4 micrometer nucleopore filter and divided by the mass of the meltwater filtered to establish an approximation of the concentration of black carbon in ng C gm^{-1}.

To create the reference standards 80 ml of filtered H_2O was added with 20 ml isoprophyl alcohol and mixed with a predetermined amount of India ink. The

relationship of the liquid mixture to India ink is shown in Table 1. In the case of reference standard number 1 – 6 the mixture was then diluted by a factor of four. Detailed discussion on the creation of reference standards is presented elsewhere (Clarke et al., 1987). Stephen Warren, University of Washington, provided the reference standards that were used in this research.

To establish this initial estimate of mass impurity concentration the air dried samples were compared to the filter reference standards. Visually comparing a sample filter to a reference standard is a subjective assessment due to the importance placed on visual acuity of the substrate saturation regardless of the filter hue. The hue of the filter can range from light grey to brown or red which indicates carbon-based or dust particulates, respectively. In an attempt to accurately assess the sample filters, three individuals from the Cryospheric Research Group at Texas A&M University evaluated the sample filters and selected the reference standard that closest matched the sample filter in saturation of impurity. To improve comparison accuracy the sample standards and reference standards were both placed on a white diffusing background (Grenfell et al., 2011). Each individual recorded their observation of the reference standard number that closest matched each sample filter. Once the observations of each individual were recorded, the reference standard numbers were converted to the corresponding mg BC cm^{-2} and averaged to determine the initial estimate of mass impurities concentration for each sample filter. Previous research comparing visual estimates to photometric analysis of filters shows that visual assessments may be in error by as much as a factor of two (Grenfell et al., 2011).

Table 1. Reference standards relationship of liquid mixture to India ink.

Reference Standard Number	**Filtered H_20 (ml) / Isoprophyl Alcohol (ml)**	**India Ink (ml)**	**mg BC cm^{-2}**
1	80/20	4.42	0.22*
2	80/20	6.25	0.31*
3	80/20	8.84	0.44*
4	80/20	12.5	0.63*
5	80/20	17.7	0.89*
6	80/20	25	1.25*
7	80/20	35	1.75
8	80/20	50	2.17
9	80/20	71	2.54
10	80/20	101	3.61
11	80/20	141	5.04
12	80/20	200	7.14

*Mixture diluted by 4x

4.3 Filter Photometric Analysis

The filters were later transported and measured photometrically during a visit to the University of Washington in Seattle in August of 2008 with a spectrophotometer using an integrating sandwich (ISW) method (Clarke, 1982b) together with an integrating sphere (IS) method, known as an ISSW spectrophotometer (Grenfell et al., 2011), to establish the averaged loading measured in ng C gm^{-1} based on the transmittance spectrum of each filter. The ISW method is designed to minimize the effect of scattering so the measured signal only accounts for losses due to light absorption (Doherty et al., 2010). The ISSW spectrophotometer has been described in detail in Grenfell et al. (2011) and is summarized here:

> The ISSW spectrophotometer uses white light illumination transmitted into an integrating sphere from an optical fiber to produce a diffuse radiation field at the output port of the sphere. This diffuse radiation then passes through the sample filter to the upper diffuser. The upper diffuser reflects and produces diffuse radiation back towards the sample filter. This causes the filter to be diffusely illuminated from both sides. The upper diffuser has an approximate reflectivity of 0.95. The absorption signal is enhanced because of multiple reflections of the radiation through the sample filter located between the upper diffuser and the integrating sphere due to the high reflectivity of the integrating sphere. The reported reflectivity of the sphere is 0.99. The radiation transmitted through the

diffuser is transmitted to a spectrophotometer where the resulting spectrum is recorded on a laptop computer (Grenfell et al., 2011).

In this study, the visible wavelengths (400 – 799 nm) of the electromagnetic spectrum were recorded by the spectrophotometer. From the measured signal, filter loadings are calculated based on fits to spectra from a set of standard filters, developed by Thomas Grenfell, that were measured by the University of Washington on February 6th, 2008.

This set of standard filters contains weighed amounts of BC. The black carbon for the standard filters is made from Monarch-71 soot and is pre-filtered to produce a size distribution similar to atmospheric BC. These standard filters are used to calibrate the system for conversion of the measured signal to a black carbon loading (Doherty et al., 2010). The conversion of the measured signal to a black carbon loading outputs a single loading value in mg BC cm^{-2} of the filter for each 25 nanometer (nm) increment of the visible portion of the electromagnetic spectrum (400 – 425 nm, 426 – 450 nm, etc.). These calculated loadings for each 25 nm increment are then averaged to produce an average loading across all wavelengths in mg BC cm^{-2} of the filter. An average loading was also calculated across 600 – 700nm where black carbon aerosol light absorption is strongest. To convert the average loading across 600 – 700 nm from mg BC cm^{-2} of the filter to ng C gm^{-1} the following equation was used:

$$loading_{average}\,(ng\ C\ gm^{-1}) = mg\ BC\ cm^{-2} \times exposed\ filter\ area \times 10^{7} \quad (1)$$

This provides a loading in ng C gm^{-1} for each sample filter. This loading is used in the remainder of this analysis.

4.4 Spectral Albedo Measurements

Spectral albedo measurements were collected to determine the effect that snow impurities have on spectral albedo and to compare these measurements to the computed spectral albedo of pure snow. A Field Spec 3 scanning portable spectroradiometer manufactured by Analytical Spectral Devices (ASD) was used to take spectral measurements. The instrument covers the visible near-infrared portion of the electromagnetic spectrum as it measures spectra between 350 nm and 1050 nm (ASD Incorporated, 2008).

This instrument was used to measure snow reflectance, radiance, and irradiance. Spectral albedo is measured most accurately under overcast sky, because then the tilt errors, due to departure of the plane of the instrument or snowpack surface from horizontal, are minimized, and the cosine errors for upward and downward irradiance cancel each other. All observations for these field campaigns were collected between 10:00 and 14:00 to coincide with the MODIS overpass for this region. These measurements are not presented in this thesis.

4.5 Ancillary Measurements

Snow density as a function of depth is required because the optical depth of a snowpack is proportional to the liquid-equivalent depth, not the geometric depth. Density is measured with a snow density kit. These measurements include snow depth measured by a depth probe and snow volume and snow weight measured using a snow tube and a slide balance. Surface temperature of the snowpack was also collected.

Additionally, snow grains were photographed by macro-photography to determine the effective optical grain size for snow model measurements.

Snow depth in centimeters (cm) was derived by using a snow depth probe at each sample site. The snow depth probe was inserted perpendicular to the horizontal surface of the snowpack and pushed through the snowpack until the depth probe met ground or ice. Each sample site was probed three times to ensure an accurate average measurement. Care was taken so that the probe did not measure dense layers of depth hoar present at some sites, but at the horizontal plane of the ground or ice. The three readings from each sample site were then averaged to calculate a composite snow depth in cm.

Snow volume depth was recorded *in situ* by using a plastic cylindrical snow tube that has depth measurements in centimeters listed on the side of the tube similar to a ruler. The snow weight was then calculated by hanging the snow tube on a sliding balance and the weight was recorded in grams. To execute this process, the empty snow tube was weighed before each sample to ensure fidelity of the measurement technique and to establish a baseline weight of the snow tube. The cylindrical snow tube was then inserted perpendicular to the horizontal surface of the snowpack and pushed through the snowpack until the snow tube met ground or ice. Snow was then removed parallel to the vertical profile of the snow tube and a metal spatula was wedged between the ground and the snow tube opening to ensure that there was no loss of snow when removing the snow tube from the snowpack. A plastic cap was then placed on the bottom of the snow tube to enclose the snow. A snow depth reading was then recorded so it could be utilized

in a snow volume equation. The snow filled cylindrical snow tube was then placed on the sliding balance so the weight in grams of snow could be calculated. This value was recorded to establish an actual snow weight. The snow volume for each site was calculated with the following equation:

$$snow\ volume\ (cm^3) = \pi \times 2.65\ cm^2 \times snow\ tube\ snow\ depth\ (cm) \quad (2)$$

As previously stated, the empty snow tube weight and the snow filled tube weight were recorded *in situ*. To gain a true snow weight the empty snow tube weight was subtracted from the snow filled tube weight. This provided a measurement of the snow weight as follows:

$$snow\ weight\ (gm) = filled\ tube\ weight\ (gm) - empty\ tube\ weight\ (gm) \quad (3)$$

From these two measurements, snow density can be derived. Snow density is simply stated as:

$$snow\ density = snow\ weight\ (gm) \div snow\ volume\ (cm^3) \quad (4)$$

Once snow density was established, the SWE of the snowpack could then be determined. SWE is the snow tube snow depth in centimeters multiplied by the Snow Density as shown below:

$$snow\ water\ equivalent = snow\ tube\ depth\ (cm) \times snow\ density \quad (5)$$

As aforementioned, the optical depth of a snowpack is proportional to the liquid-equivalent depth. Evaluating the optical depth of a snow pack and the liquid-equivalent provides an increased understanding of the *in situ* sample sites as well as the snow fall event samplings as a whole.

In addition to measurements need to determine the optical and liquid-equivalent depth of the snowpack, the snow surface temperature was also recorded *in situ*. The surface temperature was recorded using a Life-Link Kit thermometer that reads the surface temperature in degrees Celsius (°). The thermometer was inserted into the snow pack at the surface next to the location of the snow sample jar. The thermometer was then left for 3-5 minutes to equilibrate. The surface temperature was then recorded in ° . These ancillary measurements have been utilized in this research to better understand the characteristics and nature of the snow fall event samplings. Selected photos of ancillary measurements are shown in Figures 10 – 14.

4.6 Snow Grain Size Analysis

Throughout the field campaign, macro photography images of snow grains were taken with a digital camera within close proximity to the sample site (Fig. 15). This was facilitated by sifting snow from the surface of the snowpack onto a snow grain card and digitally capturing a macro photography image (Fig. 16). Once the snow grain images from the field campaign were compiled, the images were processed using a public domain Java image processing program titled ImageJ (Abramoff et al., 2004). This downloadable application supports basic digital image processing and has the ability to calculate area and pixel value statistics of user-defined selections. With the assistance of ImageJ, all snow grain images are processed to retrieve the snow grain radius. The image processing steps for snow grain analysis are described below.

Fig. 10. Individual snow sample jar on top of snowpack.

Fig. 11. Snowpack temperature measurement.

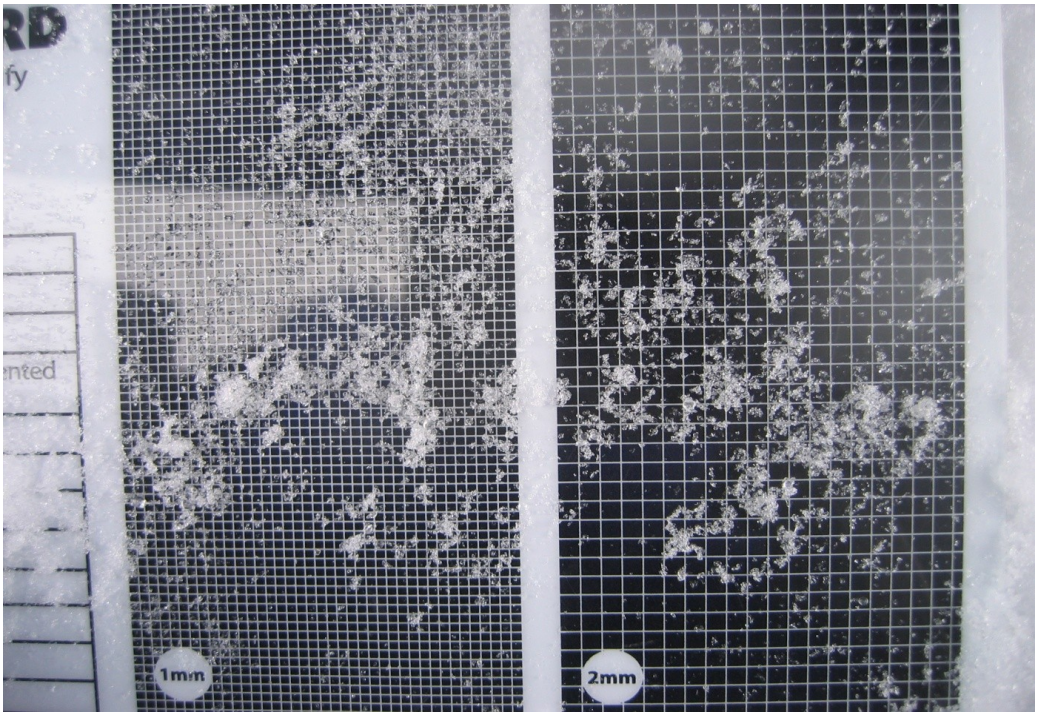

Fig. 12. Snow grain crystal card.

Fig. 13. Snow depth measurement.

Fig. 14. Measuring snow density.

Fig. 15. Example sample site for snow grain card macrophotography.

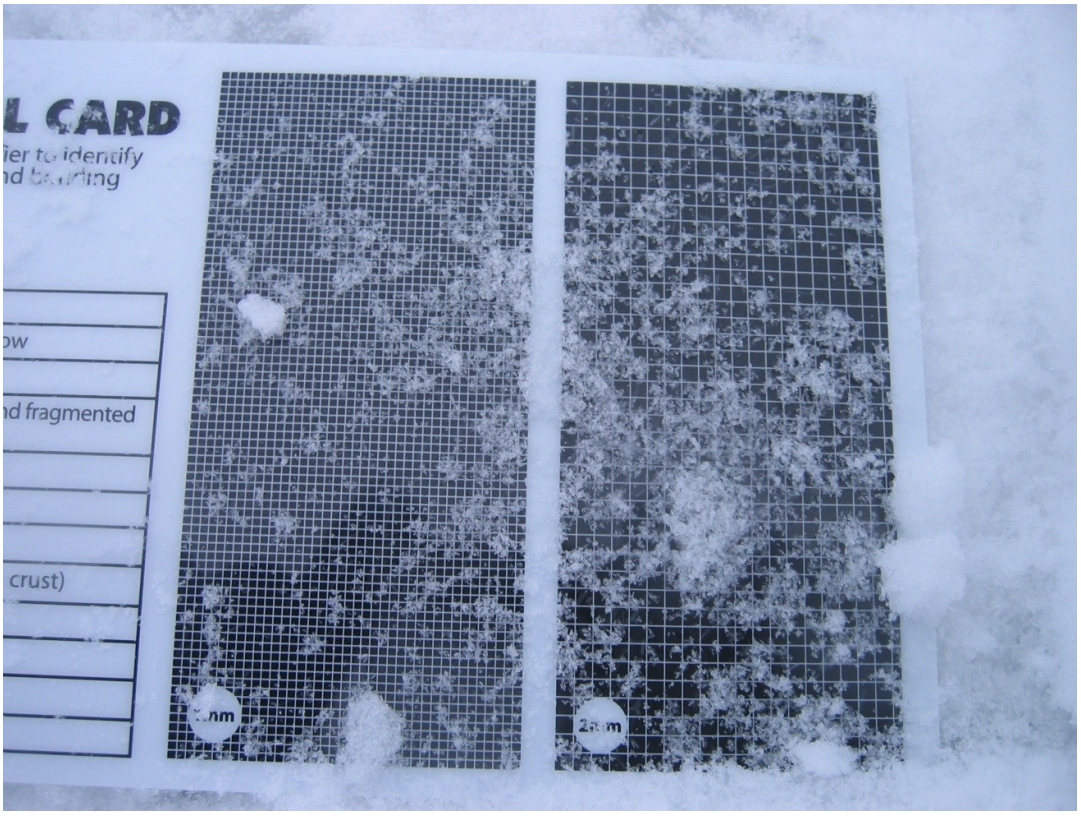

Fig. 16. Snow grain card macrophotography image.

Each snow grain image was loaded into ImageJ and the image went through a five step process that included image sharpening and enhancing contrast, making the image binary, selecting grains through visual acuity, analyzing particles, and determining snow grain radius.

Sharpening the image increases contrast and detail, but also can adversely accentuate noise. The sharpening filter used weighting factors to replace each pixel with a weighted average of the 3x3 neighborhood. The image then underwent contrast enhancement that increases image contrast by histogram stretching but did not alter the pixel value. After this pre-processing step was completed the image was then transformed into a binary (black and white) image (Fig. 17). The threshold level for this step was determined by an automatic thresholding function that divided the image into objects and background by establishing a test threshold and computed the average of the pixels at or below the threshold and pixels above. Next, the software then computed the average of the pixels at or above and below the threshold value, and then the threshold was incremented and the process was repeated. Iterations of this process were stopped when the threshold was larger than the composite average.

In step three of this process snow grains were selected through visual acuity. Before selection, spatial calibration was applied to the image by using the measured grid block on the grain size card. The blocks on the grain image are broken up into 1 mm and 2 mm grid blocks. The spatial calibration was set using the right panel of the snow grain card where the spatial resolution of a single grid block is 2 mm. Spatial calibration is necessary to provide real world dimensional measurements.

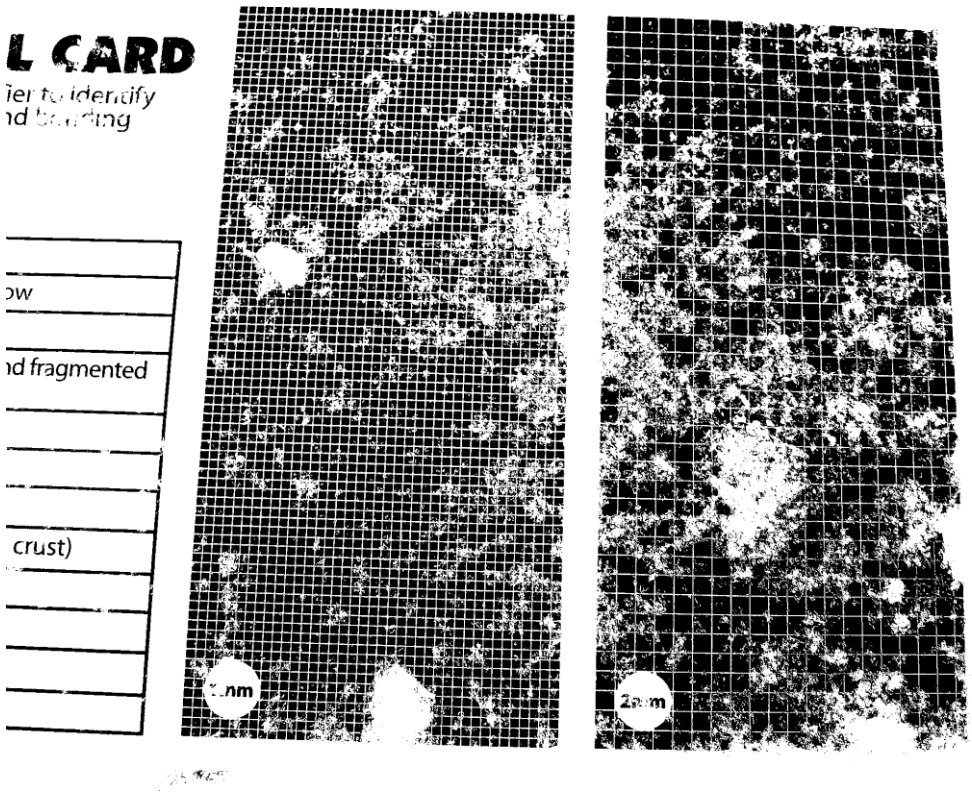

Fig. 17. Contrast and binary processing step for snow grain size analysis.

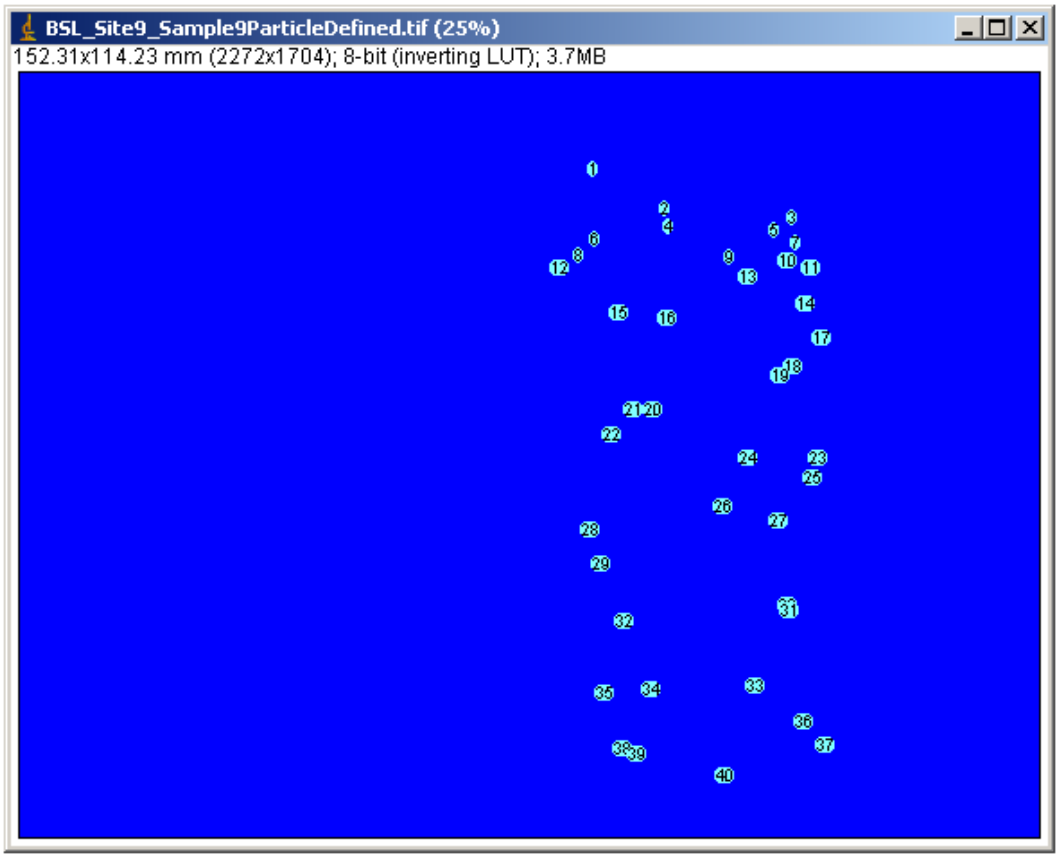

Fig. 18. Fit ellipse processing step for snow grain size analysis.

The image was scanned visually and forty grains representative of the sample were selected for analysis. The selection tool was used to create irregular area selections of the forty grains and the background of the selection, or the remaining portion of the image, was cleared. The remains were the image of only the selected forty grains to be processed during step four (Fig. 18).

Particle analysis (Step 4) was completed in ImageJ by utilizing its analyze particles macro which counts and measures the grains in the image. It completed this process by scanning the image until it found the edge of an object, outlined the object, measured the object, filled the object to make it invisible, and then resumed scanning the image until the end of the image was scanned. The analyze particles macro outputs basic statistics such as area, mean, xmin, xmax, skewness and kurtosis.

Previous research by Aoki et al. (2000) defined snow grain size as half of the minor axis of the smallest dendrite or crystal (r^2). This definition was chosen so that the algorithm and validation *in situ* measurements would be evaluated using the same methodology. Aoki et al. further confirmed previously published radiative transfer modeling completed by Warren and Wiscombe (1980) that freshly fallen snow should range from 50 – 100 micrometers. The definition presented by Aoki et al. (2000) was utilized in this research.

For each snow grain in the image the measured length of the major and minor axis of crystals or dendrites was established. The minor axis measurement, or diameter, of each individual crystal was then divided in half to determine the radius of the narrowest part of the crystal. The average radius and area of the subset of snow grains on

each image were then used to establish the optical equivalent snow grain size for each sample site.

4.7 Trajectory Modeling

Atmospheric soundings are a measurement of the vertical distribution of physical properties (e.g., pressure, temperature, wind speed, wind direction, liquid water content, ozone concentration, pollution) of the atmospheric column. Atmospheric soundings in the form of a skew-T log-P diagram were evaluated for the Iowa validation study site. These diagrams display the temperature and dew point as a function of pressure and were used to determine the vertical height of the air parcels in which the parcel of air was cooled to the point water vapor condensed. The heights at which water vapor condenses and precipitation occurs are those most likely for particulate matter to be scavenged from. Determining the vertical height of the air parcels where precipitation occurred made it possible to derive the height above ground level inputs necessary for trajectory modeling. For the snow events studied this corresponds to elevation between 500 – 1500 meters above ground level (AGL). Modeling these levels of the atmosphere where scavenged particulate matter was most likely to occur for this storm provides a better sense of where the impurities present in the *in situ* measurements has traveled from.

The National Oceanic and Atmospheric Administration and Air Resources Laboratory Hybrid Single-Particle Lagrangian Integrated Trajectory model (NOAA ARL HYSPLIT model) (Draxler and Rolph, 2003) was used to compute air trajectories using archived data from the date of each snowfall event to find possible origins of the

air parcels during the sample collection periods. Single point trajectories and trajectory matrixes were run backwards in time for 96 hours at three different heights above ground level (500 m, 1000 m, and 1500 m). A time frame of 96 hours was selected as this was the longest backwards trajectory that the model could predict.

4.8 Remote Sensing Determination of Grain size and Soot Concentration

Moderate Resolution Imaging Spectroradiometer (MODIS) radiance and surface reflectance satellite images were acquired throughout the field campaign. MODIS has a viewing swath width of 2,330 km and views the entire surface of the Earth every one to two days. Its detectors measure 36 spectral bands between 0.405 and 14.385 μm, and it acquires data at three spatial resolutions: 250 m, 500 m, and 1,000 m. MODIS images collected over the validation site during the field campaign were used in attempt to validate the ADEOS-II/GLI snow algorithm for snow grain size and soot concentration. A total of nine images taken throughout the field campaign were originally identified with clear skies that could be compared to the validation data for the period between the two snow storms. These imaged were collected on dates between February 27, 2007 and March 4, 2007.

The ADEOS-II/GLI snow products are mainly written in Fortran and require the input file data format to be binary. In return, the output file in binary data format provides pixel-by-pixel information for snow grain size and the mass fraction of soot mixed in the snow for cloud-free pixels (Stamnes, 1999a). The ADEOS-II code was originally written for image data from the Global Imager (GLI) sensor onboard the ADEOS-II platform, therefore spectral bands hard coded in the algorithm specific to the

GLI sensor were mapped to the corresponding MODIS bands so that the code could be compiled and ran on MODIS images. The GLI bands in the algorithm pertaining to snow grain size and soot concentration were GLI channel 5 (MODIS 3) and GLI channel 19 (MODIS 2). MODIS binary radiance files were used as input into the algorithm. A single MODIS image was then run through the compiled code attempting to output the grain size and mass fraction of soot mixed in the snow for cloud free pixels. Even though the code was re-written so that measured radiance values from the MODIS images could be read into the algorithm the iteration of comparing the measured radiances to simulated radiances produced null values in the binary output file.

It was apparent from the output file that the algorithm as implemented did not behave as anticipated. A summary of the actions the algorithm should have taken is summarized as follows. First, the snow grain size in MODIS channel 2 should have been adjusted until the computed top of atmosphere (TOA) radiances agreed with the measured normalized radiance. Second, the mass fraction of soot in the snow should have been estimated using the radiance of MODIS channel 3 after the grain size was determined from measurements of MODIS 2. Finally, the computed TOA radiances are compared with the measured ones in channels 2 and 3 and if the result was found to be inconsistent the code should iterate until the computed radiances agreed with the measured radiances for both MODIS channel 2 and 3.

Since the GLI code was run on MODIS images and met with no success for the soot and grain size algorithm, the Fortran algorithm was ported into Interactive Data Language (IDL) to better understand the algorithm and to enable MODIS comparisons.

Since the atmospheric conditions were known at the time the images were collected, the comparison only involved the LUT for the atmospheric profile corresponding to Mode 3 which is a rural aerosol model with a winter atmospheric profile.

The ported IDL code was also unable to uniquely identify a particular snow grain size and soot concentration that would lead to the combination of observed normalized TOA radiances from MODIS 2 and MODIS 3. However, from the ported algorithm it was possible to determine the normalized TOA radiances in GLI 5 (MODIS 3) and GLI 19 (MODIS 2) their model estimated for solar zenith, sensor zenith, and relative azimuth for the pixel corresponding to the MODIS study site for each of the image acquisitions. The results from the ported IDL code are presented here.

5. RESULTS

5.1 Iowa Impurity in Snow Results: Multi-day Monitoring Locations

A total of 36 snow samples were collected at the multi-day monitoring locations with a sample collected at each of the 12 sites during each event. Of the 36 snow samples collected across the three events of the Iowa field campaign, one filter had a bad spectrophotometer reading (Sampling 3: Site 5) and is not considered in the results provided below. The spectrophotometer used in this analysis returned the measured filter signal to high too be fit to sample standard spectra. This prohibited the measured signal from being converted into a corresponding loading for this sample.

The Iowa field campaign ran from February 25, 2007 to March 2, 2007. This campaign was comprised of three multi-day monitoring samplings (12 sites) on February 25th, February 27th, and March 2nd, respectively. The multi-day monitoring location samplings are summarized in Table 2. To illustrate these results, a side-by-side comparison of the loadings for all three samplings is shown in Figure 19. Sampling 1 occurred on February 25, 2007 and should be representative of a freshly fallen North American prairie snowpack. Sampling 1 resulted in an average impurity concentration of 23.05 ng C gm^{-1} with a range from 10.1 – 40.0 ng C gm^{-1}. Sampling 2 which occurred on February 27, 2007, was a 24 hour time-elapsed sample from the snowstorm beginning on February 25, 2007 and continuing through February 26, 2007. Sampling 2 resulted in an average impurity concentration of 40.6 ng C gm^{-1} with a range from 19.7 – 75.5 ng C gm^{-1}. Sampling 3 was representative of a second freshly fallen snowpack. Sampling 3

Table 2. Iowa multi-day monitoring sample loadings (ng C gm^{-1}).

Location	Sampling 1	Sampling 2: 24 Time Elapsed Collection	Sampling 3
Site 1	10.1	75.5	115.1
Site 2	40.0	31.6	36.5
Site 3	19.1	49.6	2.4
Site 4	26.3	21.1	6.8
Site 5	27.4	34.8	*
Site 6	23.5	50.1	32.8
Site 7	29.0	32.5	38.2
Site 8	26.2	31.5	34.7
Site 9	14.4	41.7	22.6
Site 10	11.3	19.7	19.1
Site 11	13.0	45.2	51.9
Site 12	36.3	53.9	61.3
Average:	23.05	40.60	38.31

*Filter from Site 5, Sampling 3: bad spectrophotometer reading

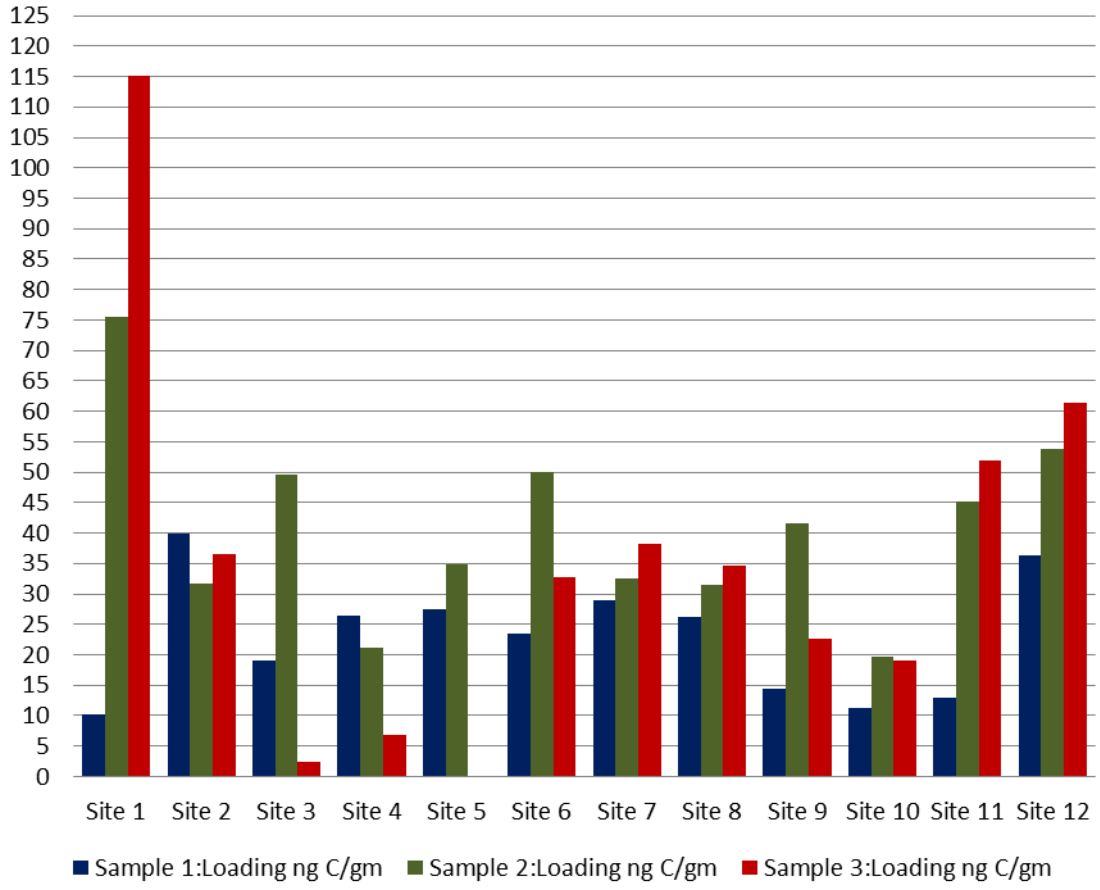

Fig. 19. Iowa multi-day monitoring samplings average loading per site by event.

which occurred on March 2, 2007, resulted in an average impurity concentration of 38.31 ng C gm^{-1} with a range of 2.4 to 115.1 ng C gm^{-1}.

Sampling 1 resulted in the lowest mean concentration of mass impurities (23.05 ng C gm^{-1}) as shown in Table 2. As the snow aged, the mass impurity concentration increased from 23.05 ng C gm^{-1} in sampling 1 to 40.60 ng C gm^{-1} in sampling 2. Sampling 2 impurity concentrations increased at all sample sites except for site 2 and site 4. Sampling 3 showed a lower mean concentration of impurities (38.31 ng C gm^{-1}) than sampling 2. However, comparison of means is not representative of the sampling as a whole. In 50% of the sites sampled, the loading increased between sampling 2 and sampling 3. Utilizing aerial photographs of Dickinson County, it became clear that sites in which the impurity concentration increased between sampling 2 and sampling 3 are primarily residential areas. Sites that decreased between sampling 2 and sampling 3 are located in the rural and lake areas of Dickinson County.

To further analyze the differences between these samplings a paired t-test and Pearson's correlation coefficient was used. This was deemed appropriate as the data is quantitative (ng C gm^{-1}), the number of samples in each data set is the same (12 sites), and the samplings are similar to a Gaussian distribution (Hill and Lewicki, 2007).

5.1.1 Sampling Statistical Results

A paired sample t-test was used to test for the statistical significance in the differences in means among all samplings for the impurity concentration variable at the 95% confidence level (Hill and Lewicki, 2007). If the significance value of the t-test was less than 0.05 then the impurity concentration variable was considered to be significantly

different between the two samplings being compared. Two comparisons were of most interest. The first was a between Sampling 1 and Sampling 2 which represent a freshly fallen snowpack and a 24 hour time-elapsed sampling, respectively to see if how, if at all, impurities increased with time since snowfall. Additionally, Sampling 1 and Sampling 3 were examined to determine if there was a significant difference in mass impurities in snowpacks deposited by two different major snowfall events.

There is a statistically significant difference (p = 0.013 at α = 0.95 confidence level) between Sampling 1 and Sampling 2. The impurity concentration for Sampling 1 had a mean of 23.05 ng C gm^{-1} with a standard deviation of 9.69 where Sampling 2 had a mean concentration of 40.08 ng C gm^{-1} with a standard deviation of 15.58 when n = 12 (representing the number of multi-day monitoring stations), this represents an averaged 43% increase in impurity concentration between Sampling 1 and Sampling 2. The Pearson's correlation coefficient (a value ranged from -1.0 to +1.0 where the closer the value is to +1.0 or -1.0 the more closely the variables are related and the closer the value is to zero there is no relationship between the variables) for this pair, Sampling 1 and Sampling 2, is -0.262.

However, there is not a significant difference present (p = 0.253 at α = 0.95 confidence level) between Sampling 1 and Sampling 3, representing separate events of freshly fallen snowpacks. The impurity concentration for Sampling 3 showed a mean of 35.13 ng C gm^{-1} with a standard deviation of 31.488 when n = 11 (the number of multi-day monitoring stations with sampling 3: site 5 excluded from analysis). The Pearson's

correlation coefficient for this pair, Sampling 1 and Sampling 3, is -0.190. Therefore there is close to no relationship between this set of samplings.

5.1.2 Spatial Results

The spatial distribution of the three samplings is illustrated in a bar graph and graduated symbol maps in Figures 20 – 23. There does not appear to be any relationship between the measured sample loadings and proximity to anthropogenic sources. In this case, the most likely anthropogenic effects are coming from either vehicle and snowmobile emissions, or wood burning stoves and fireplaces. However, in this study rural and residential areas appear to have similar snow impurity concentrations for freshly fallen snow for the events studied.

5.1.3 Trajectory Results

The atmospheric soundings used as input to the HYSPLIT trajectory model show that any precipitation would most likely occur in the atmosphere between 500 and 1500 meters AGL. Precipitation scavenges particles from the atmosphere which adhere to the snowflakes as they fall. The HYSPLIT trajectory model runs provide insight into where the *in situ* measured snow impurities could have traveled from in the 96 hours preceding the scavenging event.

HYSPLIT trajectory modeling showed similar 96 hour backwards trajectory for all three samplings (Figs. 24 – 26). The HYSPLIT backwards trajectory modeling for sampling 1 (Fig. 24) showed comparable trajectories for 500 and 1000 meters above ground level (AGL) with greater deviation at 1500 meters AGL.

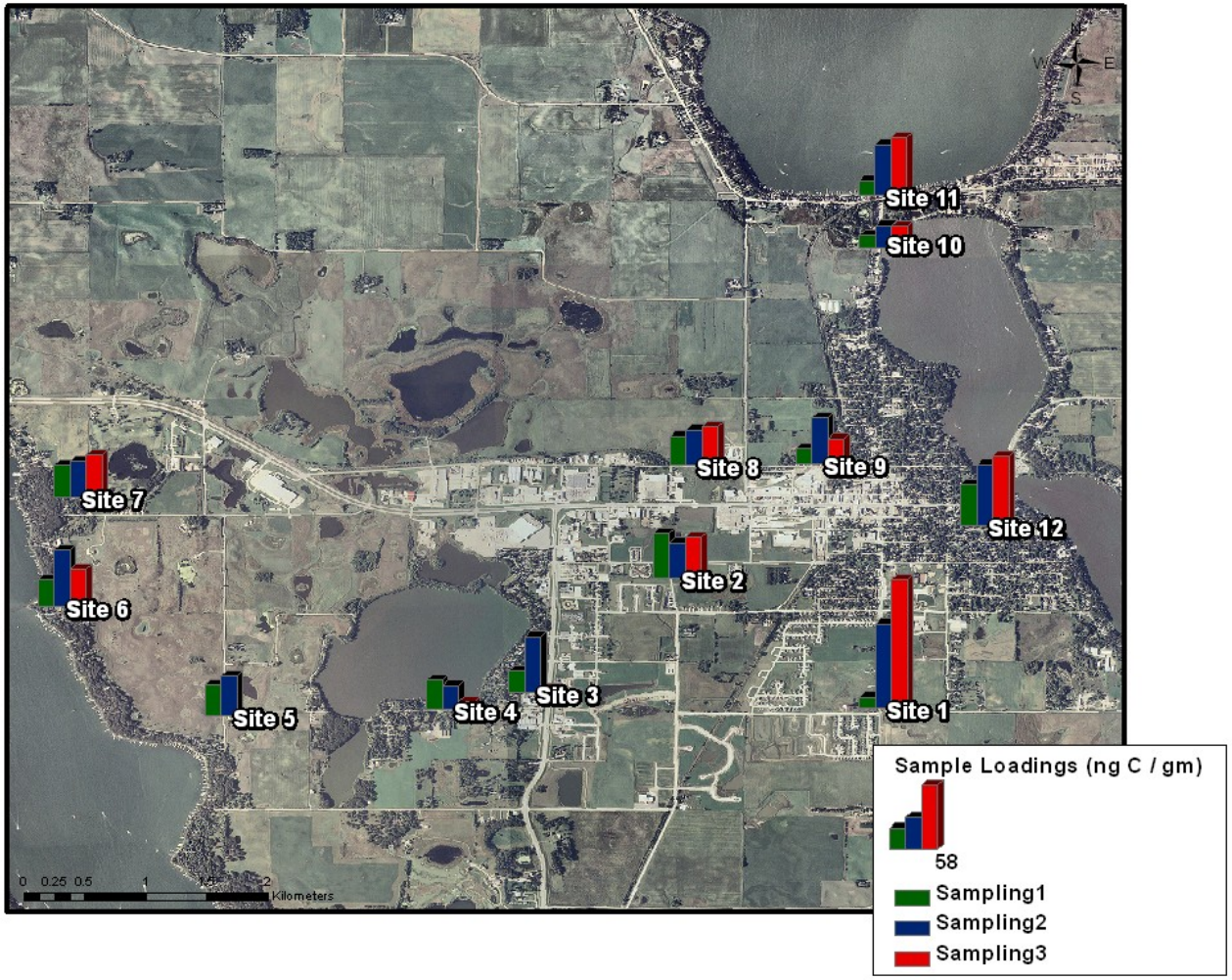

Fig. 20. Multi-day monitoring site bar graph loadings map.

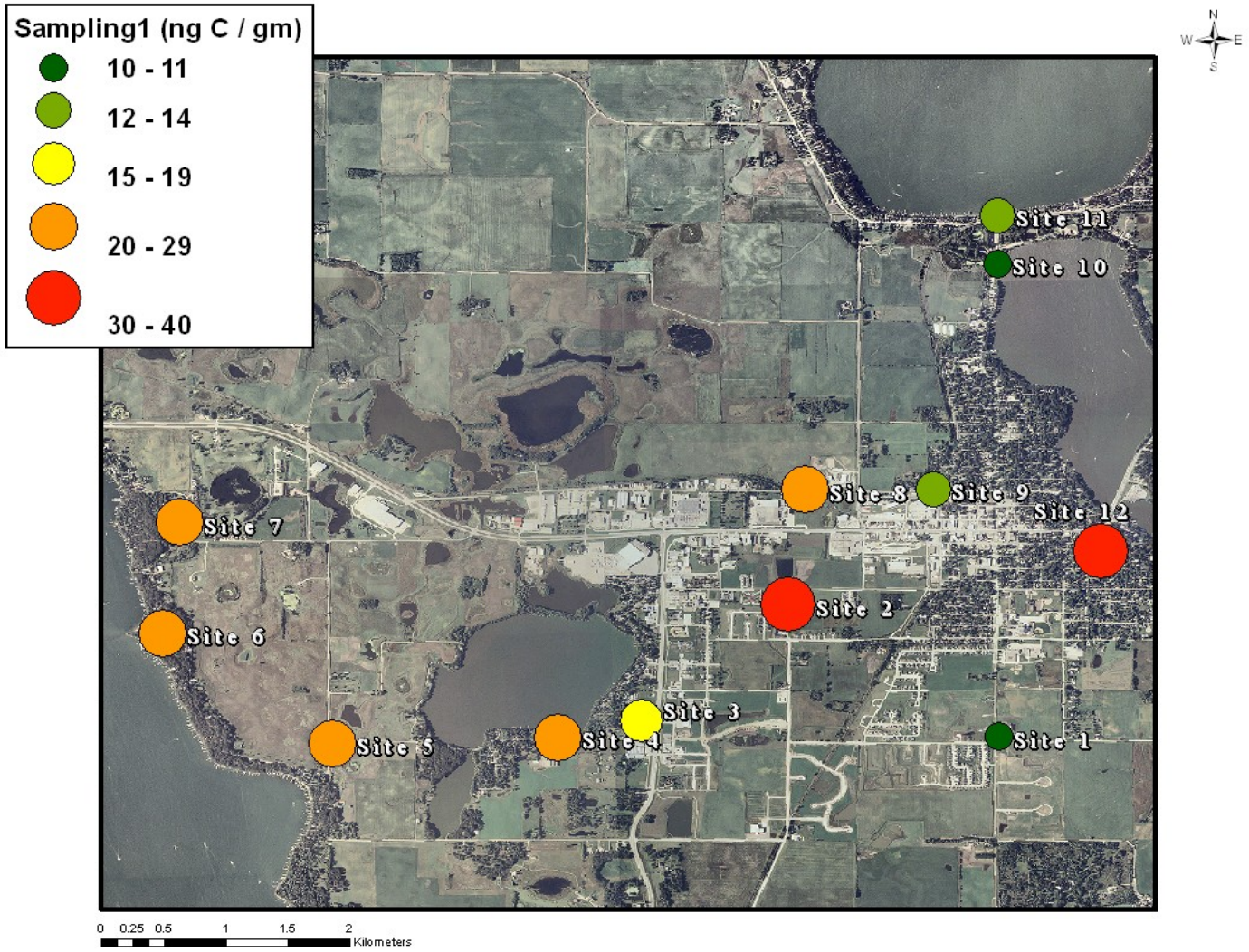

Fig. 21. Iowa sampling 1: loadings for the first snowstorm event.

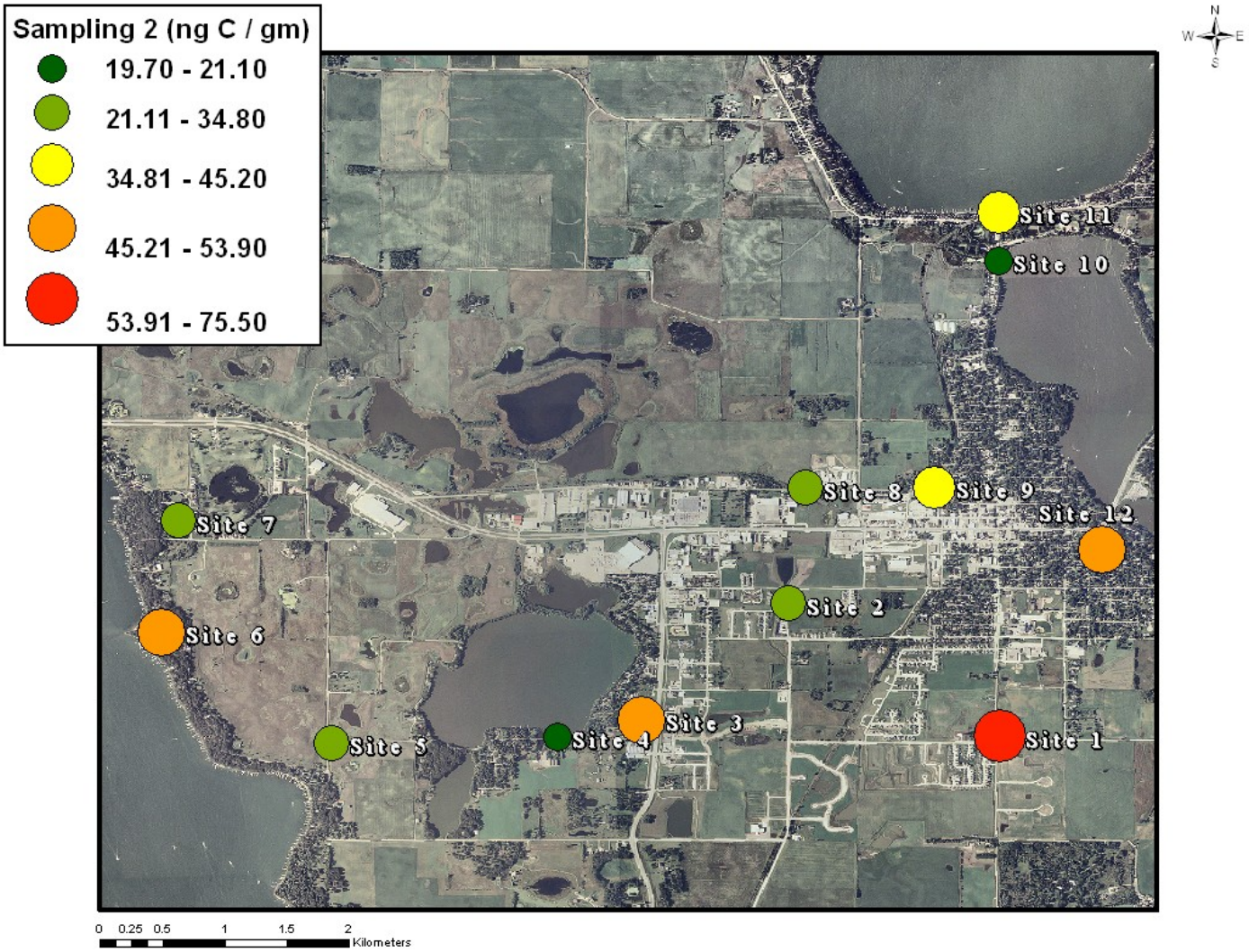

Fig. 22. Iowa sampling 2: 24 hour time-elapsed collection.

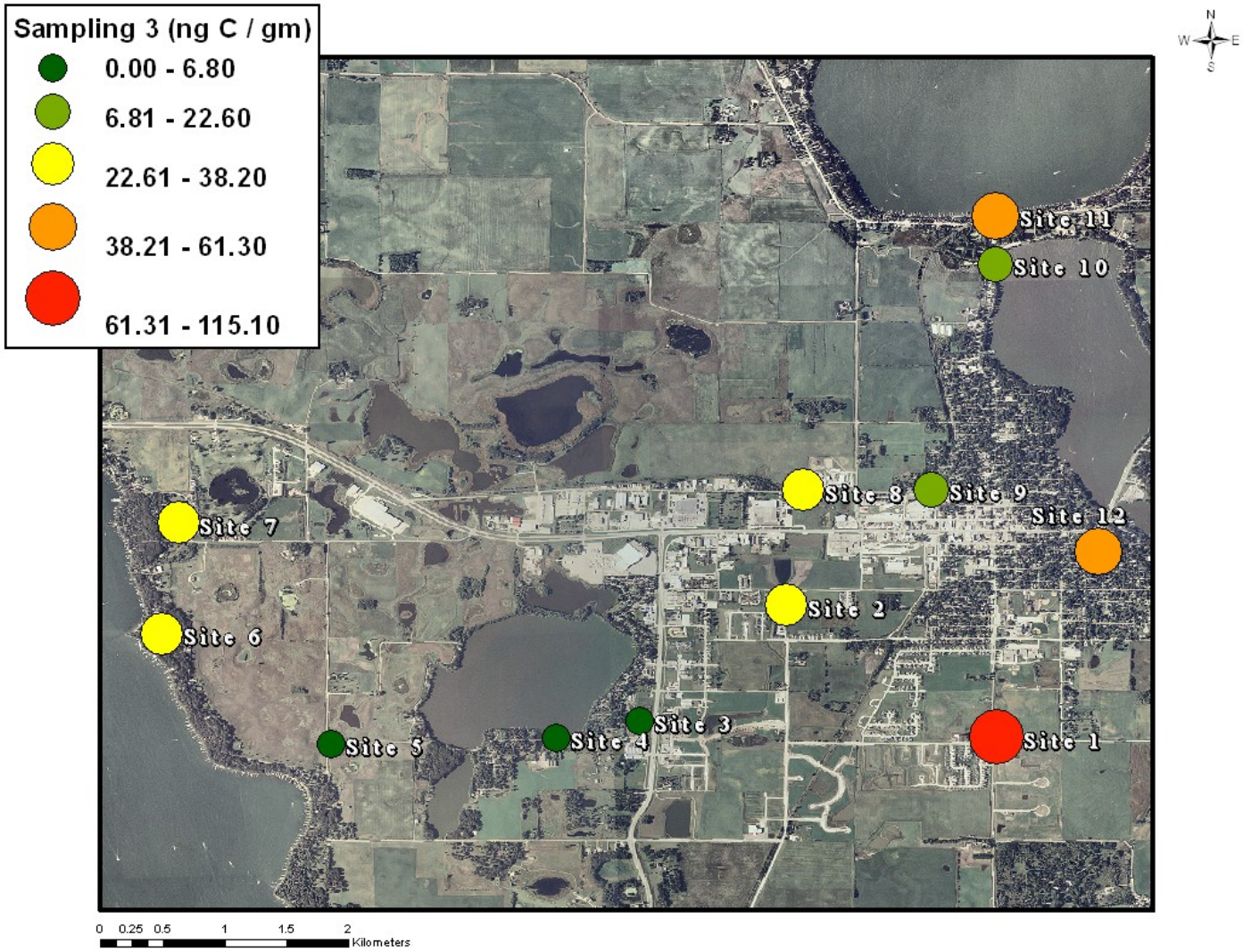

Fig. 23. Iowa sampling 3: loadings for the second snowstorm event.

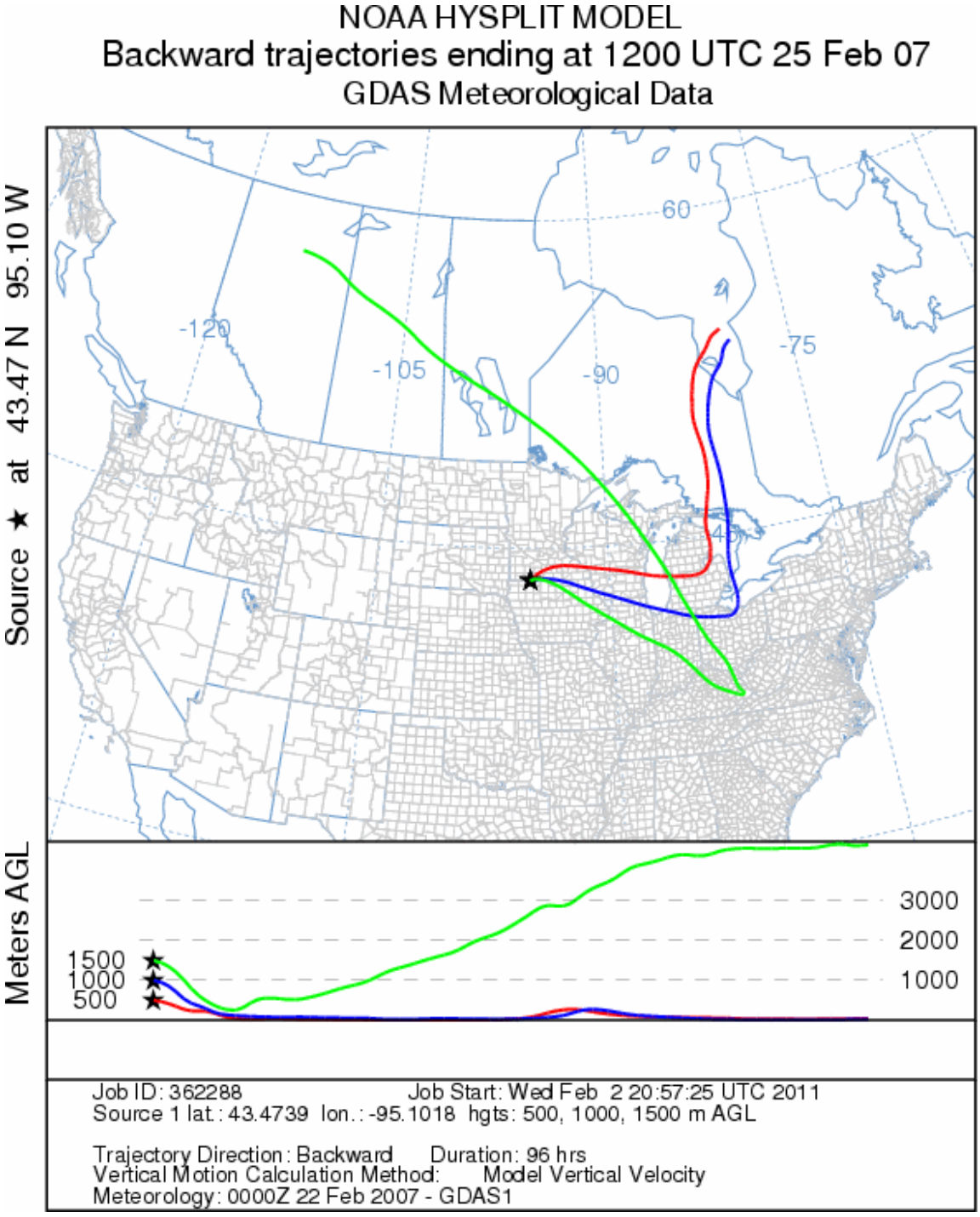

Fig. 24. Sampling 1 HYSPLIT trajectory model.

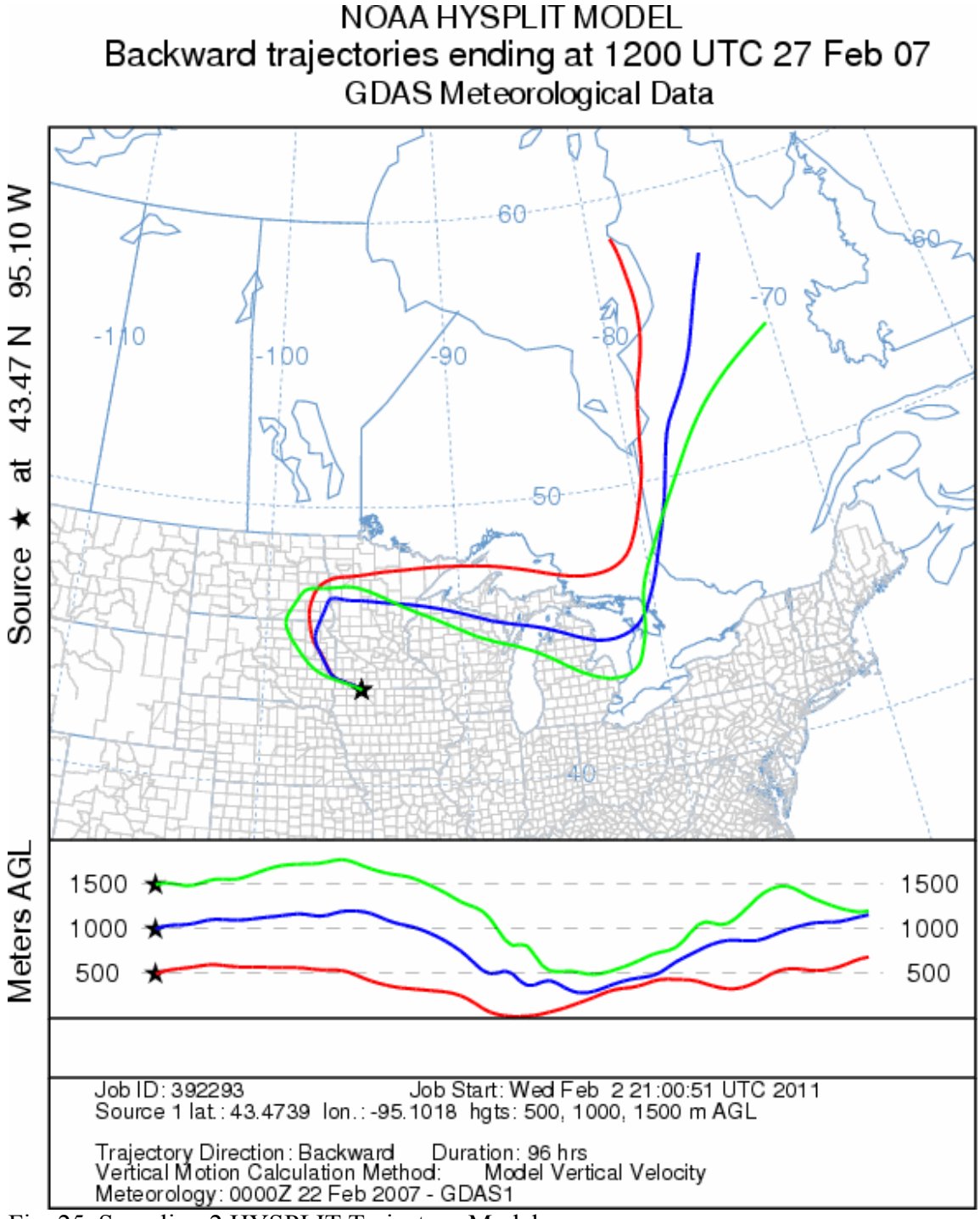

Fig. 25. Sampling 2 HYSPLIT Trajectory Model.

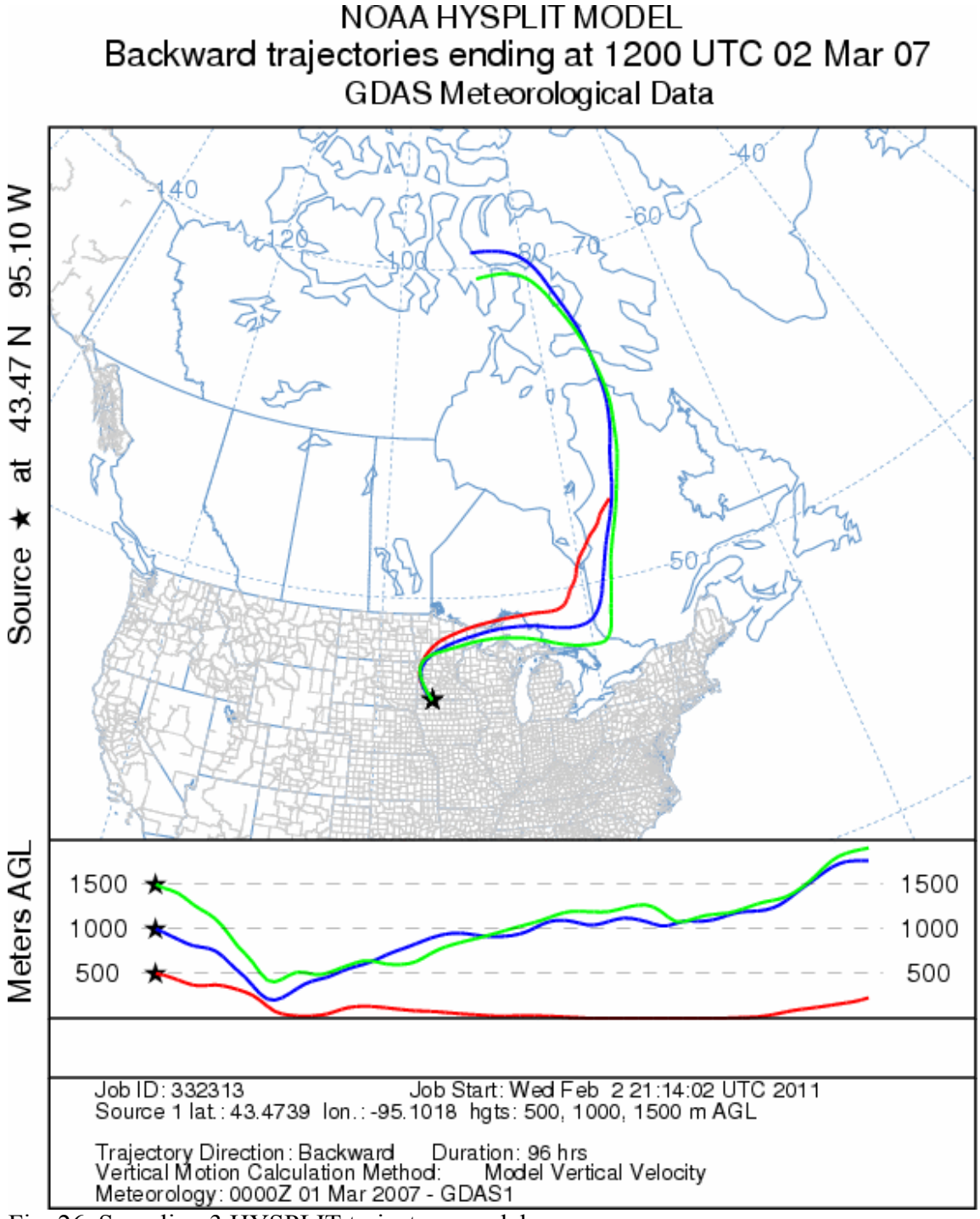

Fig. 26. Sampling 3 HYSPLIT trajectory model.

Trajectories at 500 and 1000 AGL showed that in the preceding 96 hours before the samples were collected on February 25, 2007 the air parcels preceded south from northeastern Canada down to Michigan before moving west towards Iowa. At 1500 meters AGL the backwards trajectory shows the air parcels at this height moving southeast from mid-northwestern Canada to as far as Kentucky and West Virginia before pivoting directions and heading northwest towards Spirit Lake, Iowa. Impurities scavenged from all heights AGL from this sampling have starting points in northern Canada; 500 and 1000 meters AGL trajectories initiating from Hudson Bay with the 1500 meters AGL trajectory initiating from Alberta, Canada.

The HYSPLIT trajectory model from sampling 2 (Fig. 25) illustrates that the 96 hour backwards trajectory begins on the eastern border of Hudson Bay for 500 meters AGL and as the meters AGL increases the origination of the air parcels moves east into Quebec, Canada. All three heights AGL at which the model was ran indicate that the air parcels moved south towards the Great Lakes before changing direction to the west and proceeding as far as North Dakota. The air parcels then had a southern trajectory to South Dakota before finally approaching Spirit Lake from the east. Sampling 3 trajectory modeling (Fig. 26) followed a air parcel path very similar to sampling 2 at all established meters AGL; however, this trajectory model showed a shorter transport at 500 meters AGL beginning in Quebec, Canada with a longer transport at 1000 and 1500 meters AGL that began in Nunavut, Canada close to the Northwestern Passages. The HYSPLIT model showed that the snow impurities scavenged from the atmosphere for these freshly fallen snowpacks was likely to occur along the previously described trajectories.

5.2 Iowa Impurity in Snow Results: Big Spirit Lake Sampling

The Big Spirit Lake sampling took place during the Iowa field campaign on February 26, 2007. The sampling was representative of freshly fallen snowpack void of anthropogenic effects on the snow due to ice fishing and snowmobile traffic regulations on Big Spirit Lake. Data collected from this sampling is summarized in Table 3. This sampling resulted in an average impurity concentration of 23.8 ng C gm^{-1} with a range of 1.0 to 53.1 ng C gm^{-1}. The mean snow temperature for the Big Spirit Lake sampling was -3.34° C with a range from -1.5° to -4.0° C. The mean snow depth for this sampling was 8.04 cm ranging from 3.67 to 13.0 cm. The average snow water equivalent (SWE) for this snow sample was 1.91 cm with a range of 0.85 – 3.44 cm. These results are illustrated in Figure 27.

Snow grain size was determined for the Big Spirit Lake sampling using macrophotography and Image J processing. Snow grain size has been defined by r_1, one-half the length of the major axis of the crystal, and r_2, one-half the length of the minor axis of the snow grain, with r_2 representing the optically equivalent snow grain size for new or faceted crystals (Aoki, 2000). The optically equivalent snow grain size is provided in Table 3 in micrometers. The snow grain size for this sampling resulted in a mean of 51.64 μm and ranges from 37.1 to 79.4 μm. Published measurements for new snow range between 50 – 100 μm, so the snow grain size presented here can be considered typical for new snow. A linear regression between snow grain size and filter loading is illustrated in Figure 28. A positive correlation was found to exist between grain size and impurity concentration. The graduated symbol map (Fig. 29) illustrates

Table 3. Big Spirit Lake MODIS sampling.

Location	Snow Temperature (º Celsius)	Average Snow Depth (cm)	Snow Water Equivalent (cm)	Sample Loading (ng C gm^{-1})	Snow Grain Size (μm)
Site 1	-3.0	8.00	1.79	38.2	68.2
Site 2	-4.0	4.67	0.92	23.2	53.5
Site 3	-2.0	13.00	3.44	25.2	48.3
Site 4	-3.0	3.67	0.85	20.1	39.9
Site 5	-2.0	5.67	1.37	13.2	39.6
Site 6	-2.0	10.67	2.88	13.2	40.4
Site 7	-3.0	11.33	2.37	14.6	44.2
Site 8	-4.0	5.67	1.31	1.0	37.1
Site 9	-2.0	6.33	1.45	53.1	79.4
Site 10	-2.0	12.00	3.64	22.7	54.3
Site 11	-2.0	4.67	1.01	19.0	43.6
Site 12	-1.5	9.67	1.97	14.0	62.2
Site 13	-4.0	7.67	1.84	37.9	71.8
Site 14	-4.0	8.67	1.92	40.5	64.7
Site 15	-4.0	8.33	2.01	18.1	37.8
Site 16	-2.0	8.67	1.79	15.3	41.2
Average:	-3.34	8.04	1.91	23.08	51.64

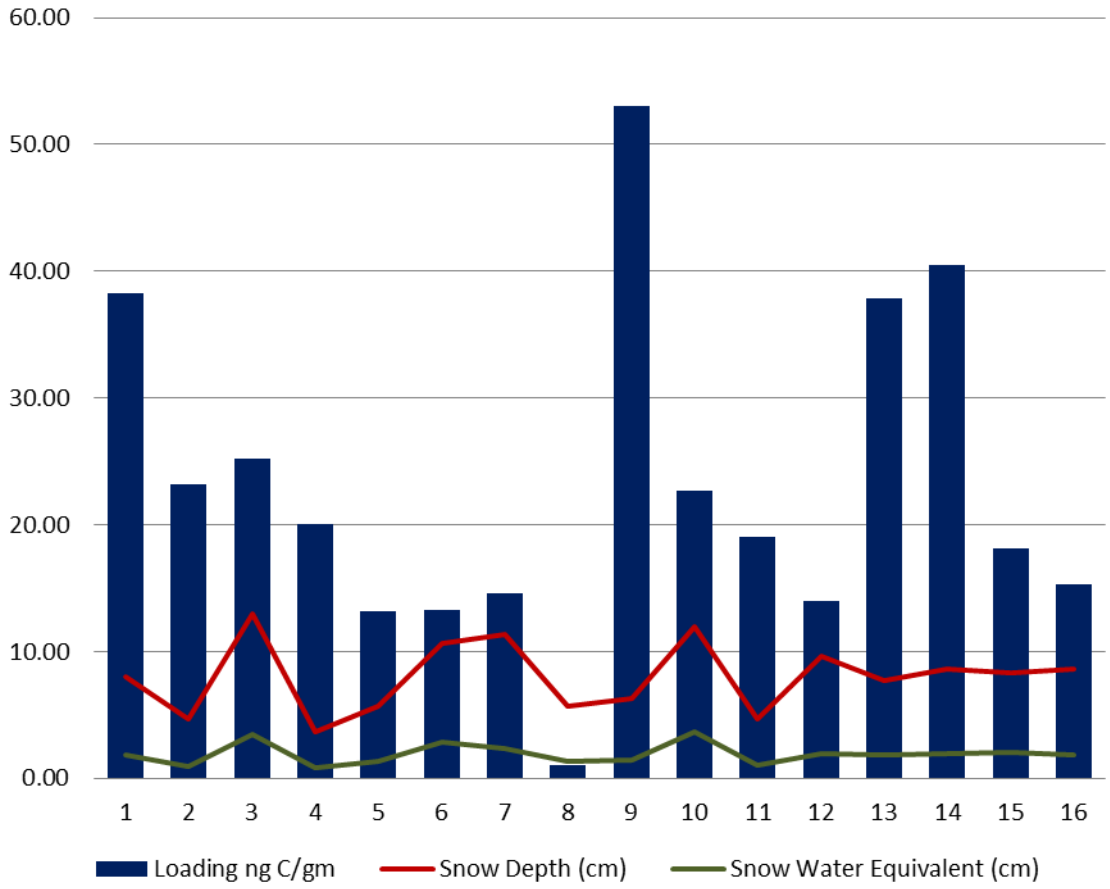

Fig. 27. Big Spirit Lake loadings.

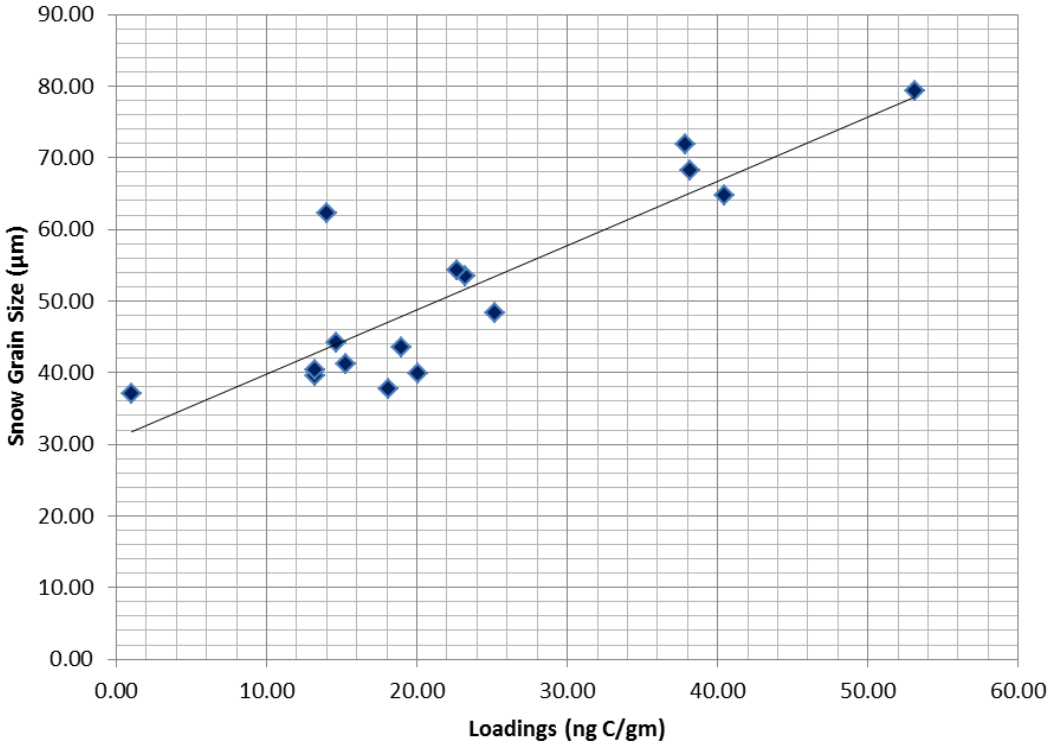

Fig. 28. Linear regression between snow grain size and loadings for Big Spirit Lake.

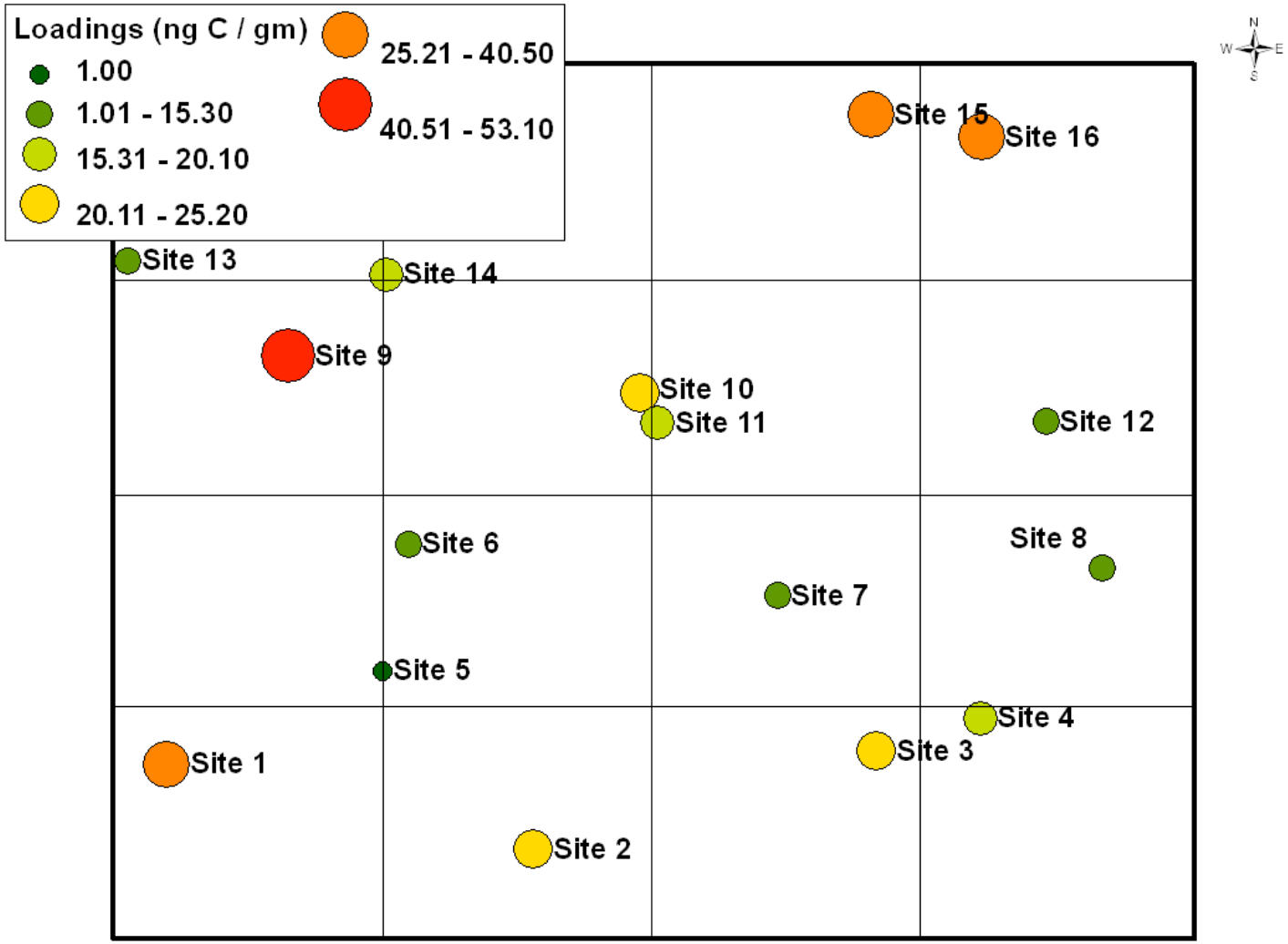

Fig. 29. Big Spirit Lake sample site loadings.

the spatial patterns of snow impurities on the sampled portion of Big Spirit Lake. No spatial patterns in snow impurity concentrations are evident.

5.3 Texas Impurity in Snow Results

The Belton, Texas sampling was collected on April 6, 2007 comprising 12 site samples from a rare and unique freshly fallen snowpack. Only one sample was collected from each site due to the increased rate of snowmelt caused by the warmer climate in this region. Impurity concentration results from this sampling are summarized in Table 4. The sampling resulted in an average impurity concentration of 56.78 ng C gm^{-1} with a range from 45.3 – 66.1 ng C gm^{-1} (Fig. 30). This freshly fallen snowpack resulted in a higher mean impurity concentration than any of the Iowa field campaign samplings. A comparison of means between this sampling and the Iowa multi-day monitoring locations showed that the Texas sampling resulted in a 146.33% increase over Iowa sampling 1 and a 48.21% increase of impurities over Iowa sampling 3. Similar to the Iowa field campaign, the spatial distribution from the Belton, Texas sampling showed no correlation between loadings and proximity to anthropogenic effects, which is illustrated in Figure 31.

5.3.1 Trajectory Results

The HYSPLIT 96 hour backwards trajectory model for the Texas sampling (Fig. 32) showed a longer transport range for 500 and 1000 meters AGL initiating from northern British Columbia, Canada on the coast of the Pacific Ocean.

Table 4. Central Texas sample loadings (ng C gm^{-1}).

Location	Loadings
Site 1	53.6
Site 2	45.3
Site 3	59.9
Site 4	66.1
Site 5	58.3
Site 6	57.8
Site 7	52.6
Site 8	49.3
Site 9	64.0
Site 10	52.4
Site 11	63.7
Site 12	58.3
Average:	56.78

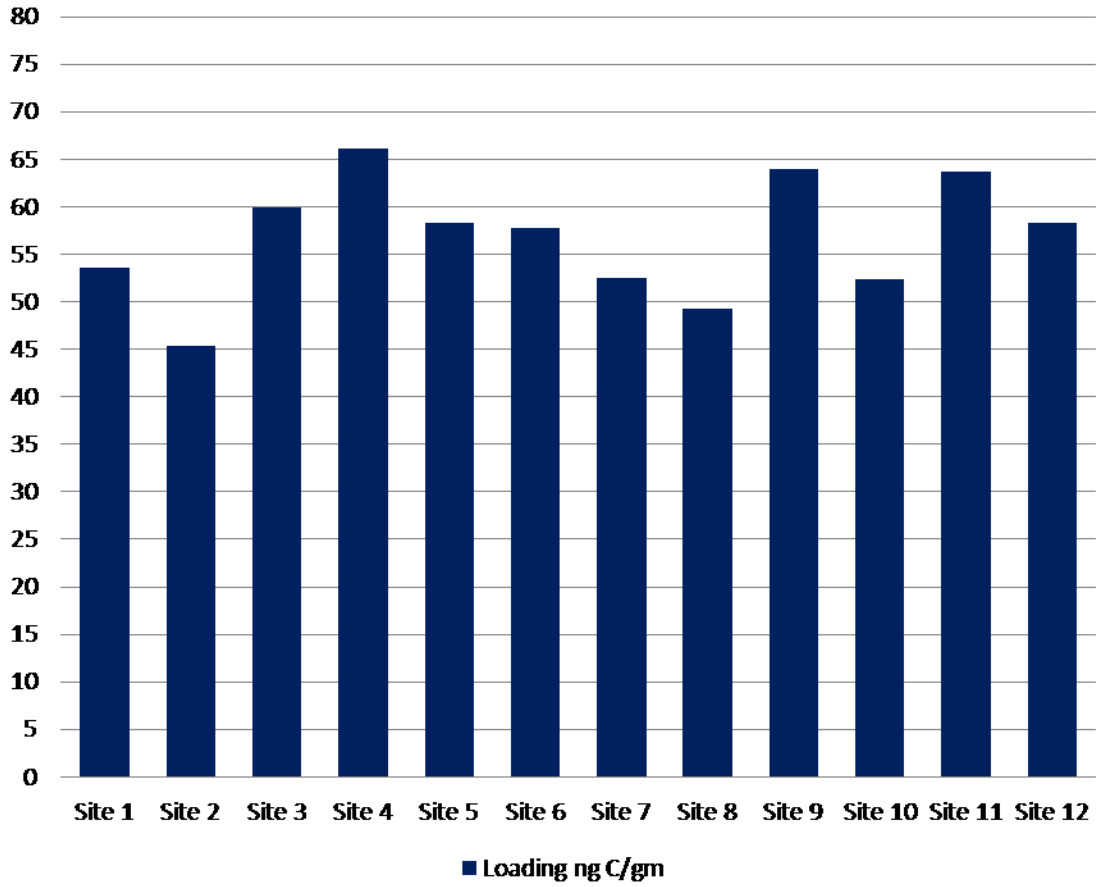

Fig. 30. Central Texas loadings.

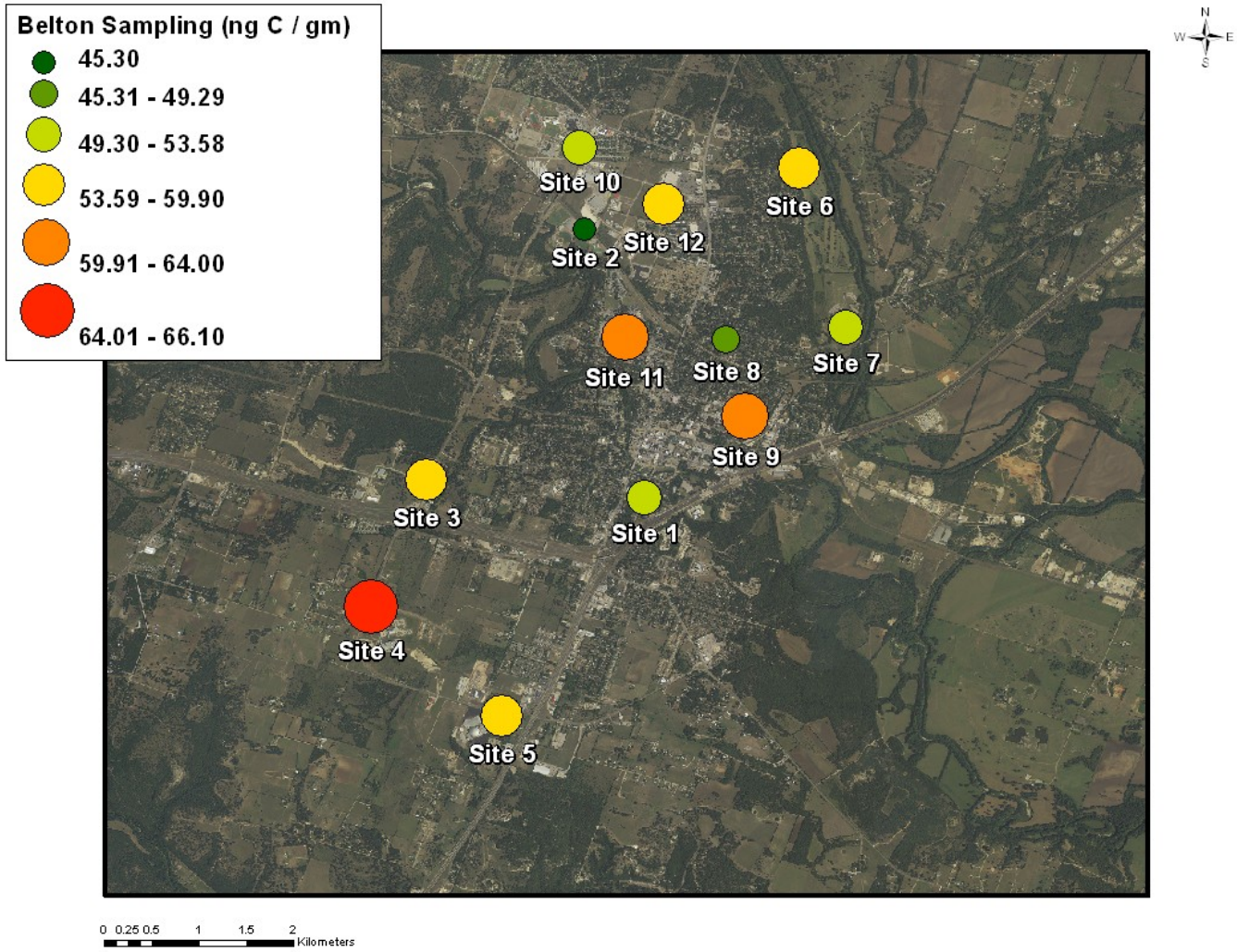

Fig. 31. Belton sample site loadings.

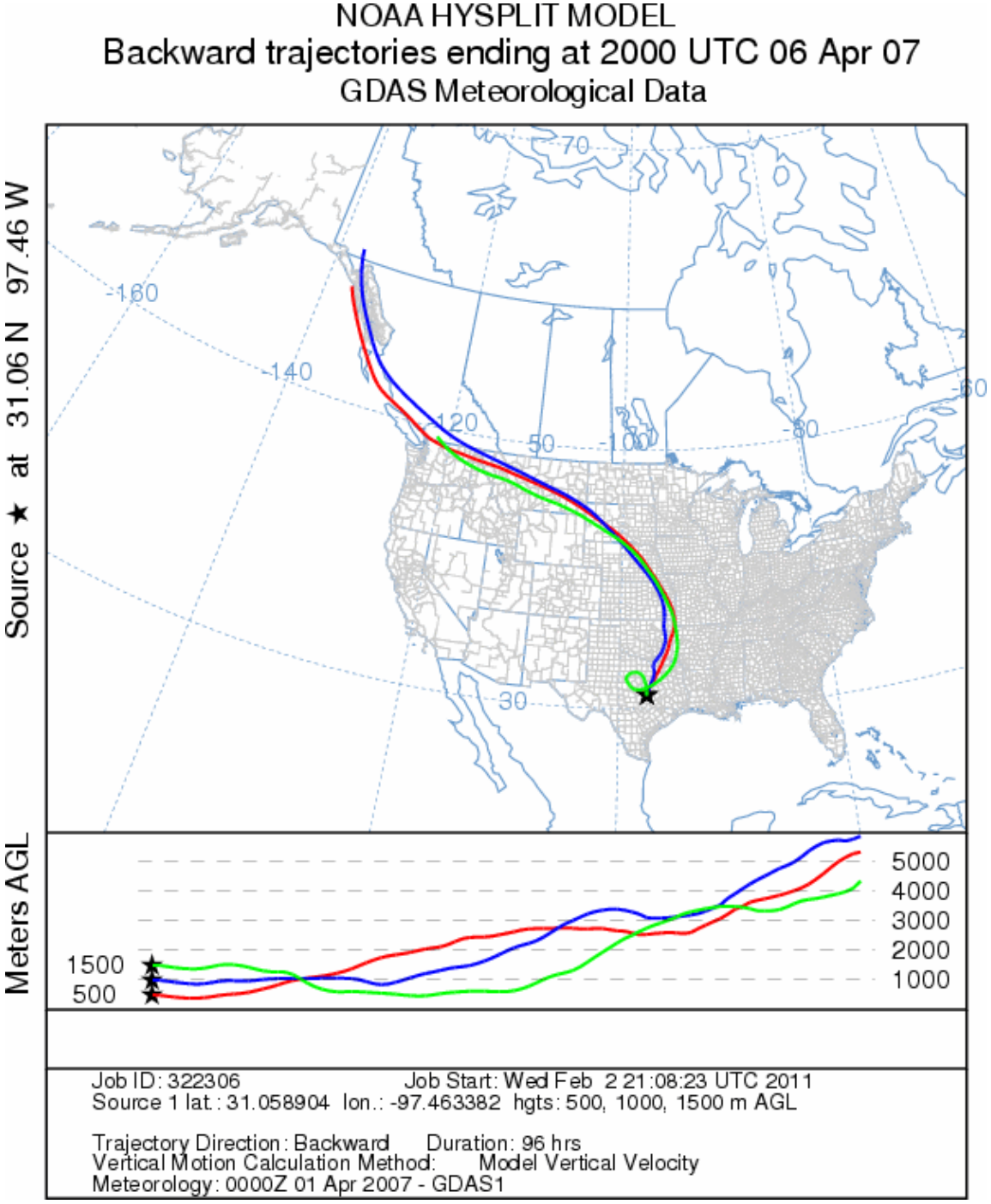

Fig. 32. Belton sampling HYSPLIT trajectory model.

Air parcel transport for 1500 meters AGL trajectory showed a shorter trajectory beginning at the border of the state of Washington and British Columbia, Canada close to Vancouver. The trajectories at all three heights AGL moved southeast towards the northeastern border of Oklahoma before heading southwest towards Belton, Texas.

5.4 Visual Assessment v. Photometric Analysis

An initial assessment of snow impurity concentrations was made by visually comparing measured sample filters to a set of reference standards with known soot concentration. At a later date, August 8, 2008, the same filters were processed in a laboratory using a spectrophotometer for a precise determination of filter loading. Research carried out on snow impurities commonly use Warren and Grenfell's set of reference standards to publish preliminary results. Quantifying the accuracy of this technique will provide confidence in the use of reference standard comparisons in future snow studies.

Subjective loadings based on visual assessment resulted in a mean of 40.99 ng C gm^{-1} with a range from 10.31 ng C gm^{-1} to 121.98 ng C gm^{-1}. Loadings assessed photometrically showed a mean of 39.71 ng C gm^{-1} with a range from 2.39 ng C gm^{-1} to 115.13 ng C gm^{-1}. The complete data set is illustrated in Figure 33. The linear regression results of all sample locations are shown in Figure 34. Statistical analysis discussed below confirms that the similar mean and range of subjective loadings and the photometric results is statistically significant.

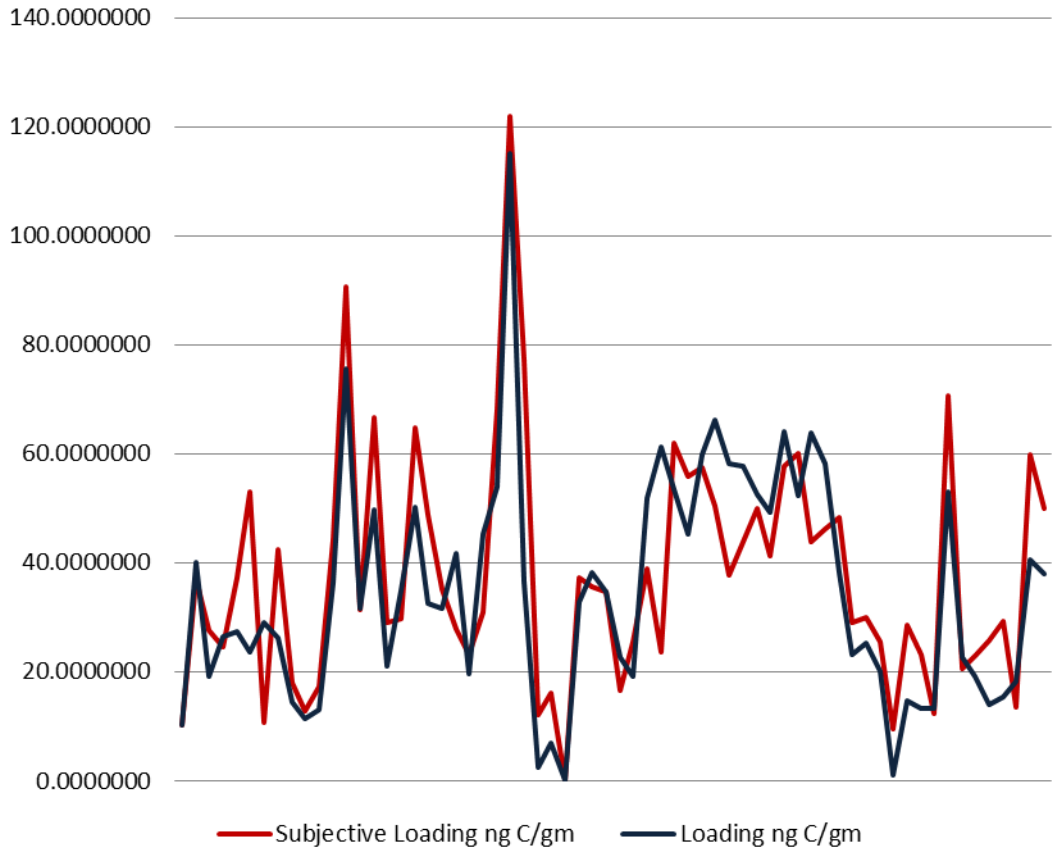

Fig. 33. Subjective visual assessments compared to photometric loadings.

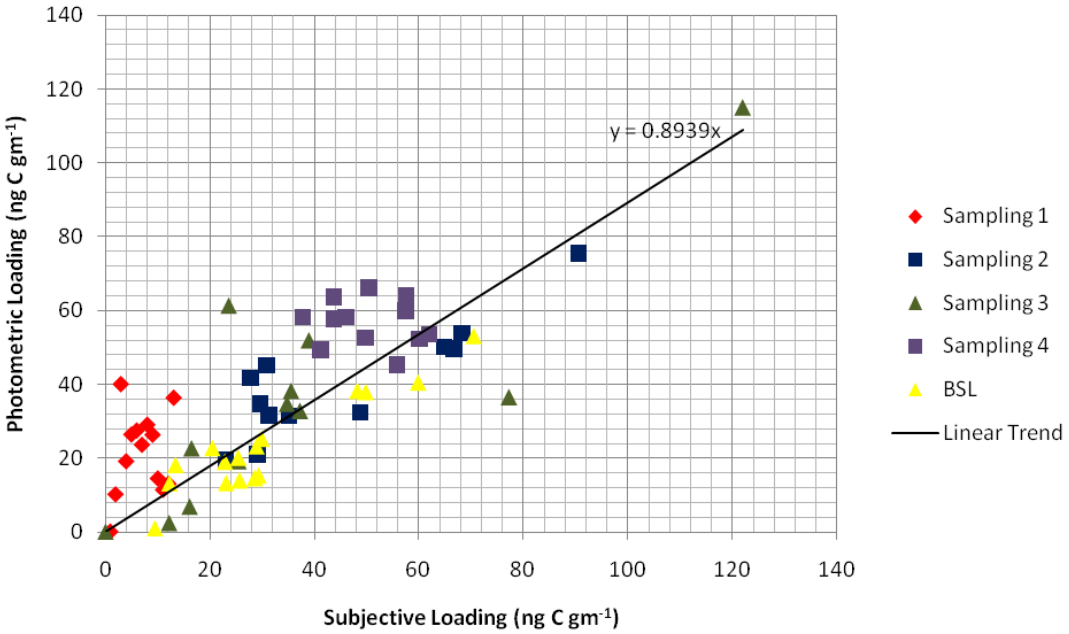

Fig. 34. Linear regression of loadings from visual assessment compared to photometric loadings.

The statistical significance in the differences in means between the filter subjective comparison loadings from the reference standards and the actual filter loading was measured using a paired t-test at the 95% confidence level. If the significance value of the t-test was less than 0.05 then the loading variable was considered to have significantly changed between the subjective comparison of the reference standard and the actual filter loading. If the significance value was higher than 0.05, then the mean for the variable was not considered to have changed (i.e., the difference between the subjective comparison of the reference standard and the actual loading would not be statistically significant). This will provide insight into the necessity of using a photometer for determining average impurity concentrations.

In analyzing the subjective loadings determined through visual acuity and the actual loadings measured using photometry, the statistical analysis indicates that there is not a statistically significant difference (significance of t-test is 0.527 at 95% confidence level) between the average soot concentrations determined though visual analysis of the filters against the set of reference standards and the average soot concentration determined using the photometer for an accurate loadings measurement. The mean impurity concentration for the subjective loadings had a mean of 40.99 ng C cm^{-2} with a standard deviation of 21.99 where actual loadings had a mean concentration of 39.71 ng C cm^{-2} with a standard deviation of 21.13. The Pearson's correlation coefficient for this analysis was 0.796 which also indicates that these two variables are closely related.

5.5 ADEOS-II Algorithm Results

The attempt to run the GLI code on MODIS images met with no success for the soot and grain size algorithm; the algorithm was ported to IDL to enable MODIS comparisons. The ported IDL code was unable to uniquely identify a particular snow grain size and soot concentration; however, from the algorithm it was possible to determine the normalized TOA radiances in MODIS channel 3 and MODIS channel 2 that the model estimated for solar zenith, sensor zenith, and relative azimuth for the pixel corresponding to the Big Spirit Lake MODIS validation site and each image acquisition.

MODIS images were acquired for collections made during the course of the field campaign between February 27, 2007 and March 4, 2007. A total of nine images of the region were originally identified with clear skies that could be compared to the validation data for the period between the two storms. A list of the nine images are shown in Table 5. The table shows each MODIS image, the date the image was collected by the sensor, and lists a reason for inclusion or elimination from this study. The validation site pixel in each MODIS image was determined to be one of the following: not located, algorithm constraint, or validated. In the case of "Not Located", the Big Spirit Lake validation site did not appear in the MODIS image and therefore a corresponding pixel was not present. A classification of "Algorithm Constraint" means that the pixel corresponding to the validation site was located in the image, but the sensor zenith angle for the MODIS image is greater than recognized angles for the GLI instrument and therefore out of the algorithms valid range. "Validation" is assigned to images in which the Big Spirit Lake validation site appeared in the MODIS image and

Table 5. MODIS images acquired for algorithm validation.

MODIS Image	*Collection Date*	*Validation Site*
2007058_1630	February 27, 2007	Algorithm Constraint
2007058_1810	February 27, 2007	Algorithm Constraint
2007059_1715	February 28, 2007	Algorithm Constraint
2007060_1620	March 01, 2007	Not Located
2007060_1755	March 01, 2007	Algorithm Constraint
2007060_1800	March 01, 2007	Not Located
2007061_1705	March 02, 2007	Not Located
2007062_1745	March 03, 2007	Validated*
2007063_1650	March 04, 2007	Validated*
*Presented and discussed in this research		

the MODIS sensor zenith angle was within the algorithms valid range.

For MODIS images 200706_1620, 200706_1800 and 2007061_1705, the MODIS validation site was not located in the images. In addition, for several of the images acquired nearest to the field sampling date, 2007058_1630, 2007058_1810, 2007059_1715, 2007060_1755 had sensor viewing azimuths greater than 45 degrees which is the limit of the GLI instrument and hence are out of the algorithm's valid range. While algorithm runs were made on the images using the highest GLI sensor zenith angle of 45° these cannot be considered accurate. The remaining two images 2007062_1745 and 2007063_1650 are presented and discussed below.

MODIS images 2007062_1745 and 2007063_1650 were collected on March 3rd, 2007 and March 4th, 2007, respectively. The results of the algorithm run on these images are illustrated as an IDL plot displaying TOA radiances that were converted to planetary albedo by standard conversions for the two spectral bands utilized in the algorithm (Fig. 35 - 36). The x-axis of the IDL plot shows expected snow grain size in micrometers for the simulated radiances (converted to planetary albedo or normalized radiance) as determined by radiative transfer modeling. The y-axis shows anticipated impurity concentration in parts per million weight for the given planetary albedo. The red region on the plot depicts an output impurity and grain size that match the measured spectral albedo (±1%). The red region shows possibilities of where the actual impurity concentration and grain size should lie for each spectral band.

A properly functioning ADEOS-II/GLI algorithm should produce a converging solution between the two bands shown in the plot. An ideal algorithm solution would

have a small area on both spectral bands where the red region is present. This would mean that the true impurity concentration and snow grain size would fall within a well defined region. In both images the algorithm solution diverged as the red region did not overlap in either case.

Additionally, not only did the solution diverge, but the algorithm results showed much higher impurity concentration and snow grain size for the measured TOA radiances than quantified *in situ* results for the MODIS validation site. These properties measured *in situ* resulted in 23.8 ng C gm^{-1} (0.0238 ppm) impurity concentration and snow grain size ranging between 39 and 79 μm. As evident in Figures 35 and 36, the algorithm retrievals would suggest much larger grain sizes and impurity concentrations. More importantly, the *in situ* quantification of both of these properties fall within previously published measurements for freshly fallen snow for both impurity concentration and snow grain size (Wiscombe and Warren, 1980).

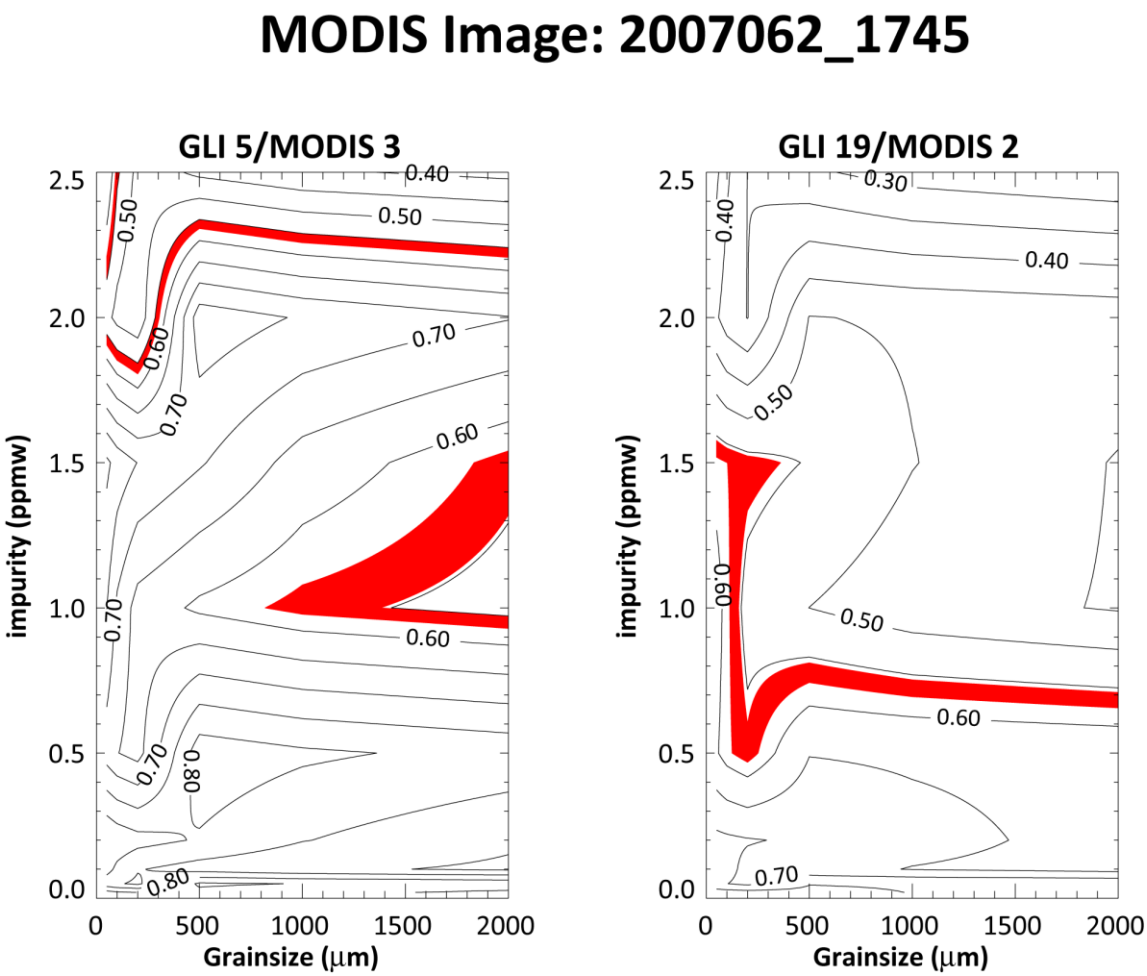

Fig. 35. ADEOS-II/GLI algorithm results for MODIS image 2007062_1745.

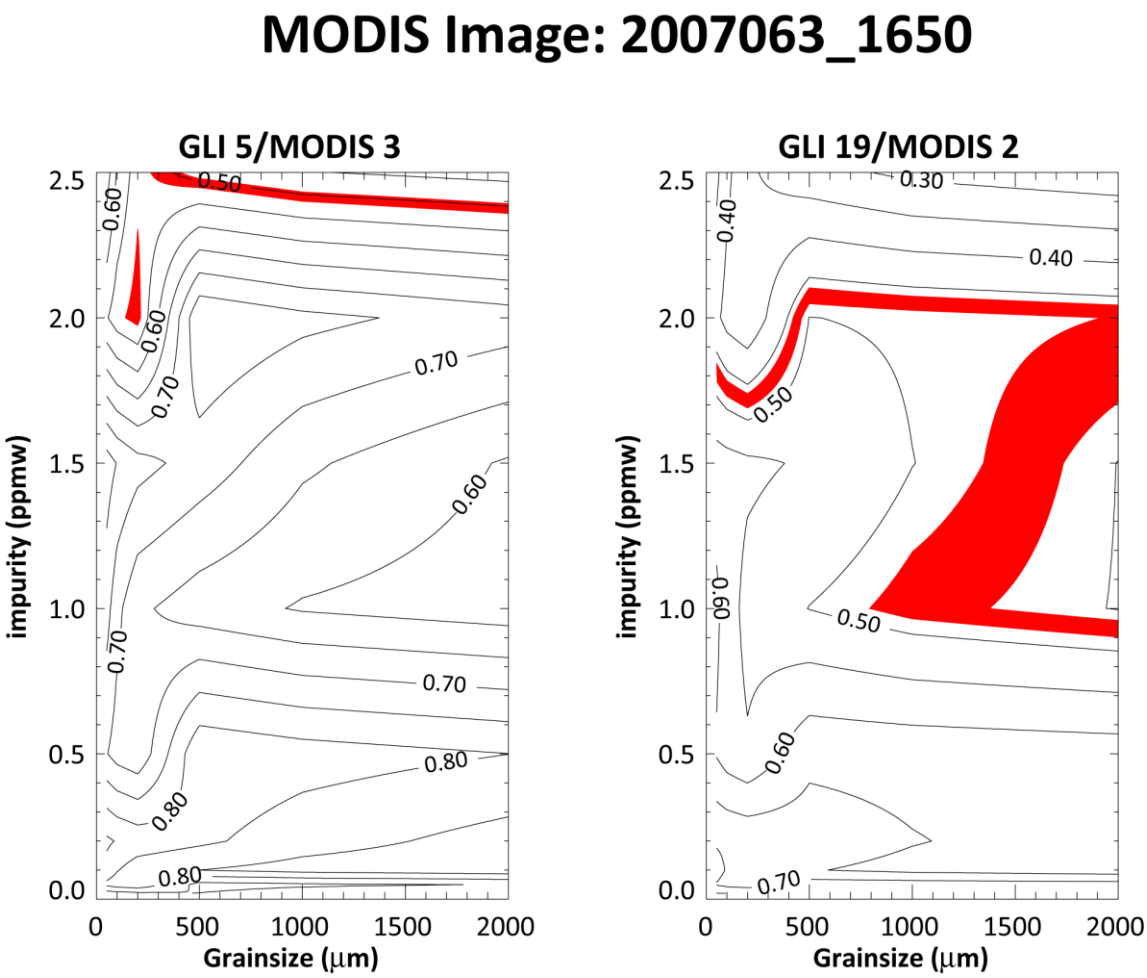

Fig. 36. ADEOS-II/GLI algorithm results for MODIS image 2007063_1650.

6. DISCUSSION

6.1 Impurities in Snow Summary

Research on impurities in snow has primarily been limited to Polar Regions and industrialized regions of China and Japan. There has been a lack of observations of soot concentrations in North American prairie snowpacks. Quantification of impurities in this region could aid future studies in determining the global effect that black carbon on has on climate. The importance of these *in situ* measurements was presented by the International Panel on Climate Change (IPCC) when they reported a low level of scientific certainty on the effects of black carbon as a RF partially due to the lack of *in situ* surface albedo measurements (Forster et al., 2007). Measuring snow properties of the freshly fallen snowpacks in Northern Iowa and Central Texas adds to the composite scientific knowledge in this field.

Measurements for freshly fallen prairie snowpacks in Northwestern Iowa and Central Texas were collected from February 25 to March 3, 2007 and April 6, 2007, respectively. Soot observations from these snowpacks indicate prairie snowpacks ranging from 1 ng C gm^{-1} to 115 ng C gm^{-1} and averaged 34.9 ng C gm^{-1}. These measurements are within range of previously published values and at amounts that can effectively lower snow albedo (Fig. 37). Impurities in North American prairie snowpacks were found to be higher than snowpacks on the Greenland Ice Sheet (Clarke and Noone, 1985), Alaska, and the Arctic Ocean (Doherty, 2010); however, the results are only slightly higher than values published for Russia (Grenfell et al., 2009).

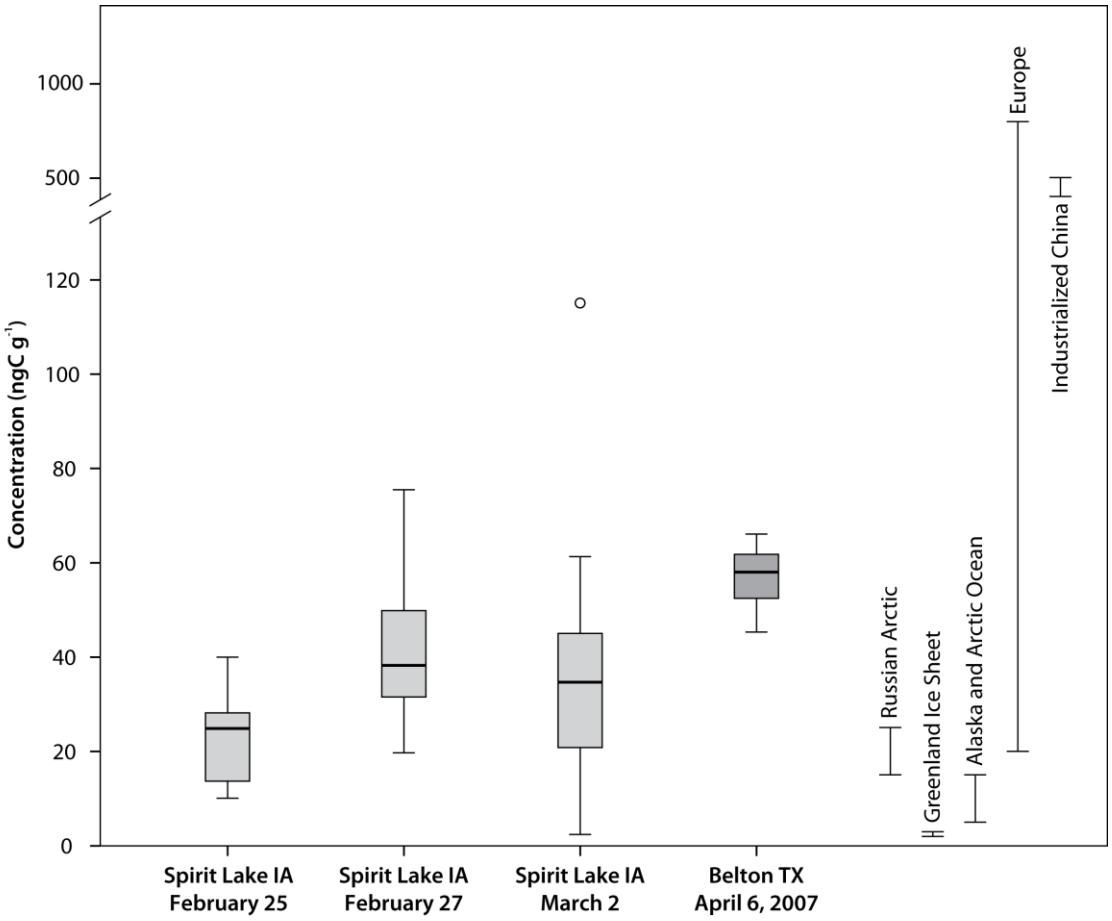

Fig. 37. Comparison of impurity concentrations for Iowa and Texas to the published literature.

Additionally, these values are within the lower range of values published for Europe, but most European values were considerably higher. Last, soot observations for North American prairie snowpack were significantly lower than values in the literature for China (Huang, 2011).

Differences in soot concentration were observed between the two Iowa snowfall events. Multi-day monitoring sites from the Iowa field campaign show that freshly fallen snow has lower impurity concentrations than aged snow. The impurity concentration between Sampling 1 and Sampling 2 increased significantly. This is of high interest considering the short amount of time (24 hours) between samplings. This agrees with the theoretical framework that Warren and Wiscombe defined through radiative transfer modeling; as snow ages the grain size of the snowpack increases and as grain size increased impurity concentration increased (Warren and Wiscombe, 1980). This research supports these findings as sampling 1 had a lower impurity concentration than sampling 2, a freshly fallen snow pack and a 24 hour time elapsed sampling, respectively. Furthermore, a statistical t-test between sampling 1 and sampling 2 confirmed that there is a statistically significant difference ($p = 0.013$ at $\alpha = 0.95$ confidence level) between sampling 1 and sampling 2.

Additional support for Warren and Wiscombe's findings is demonstrated by the mean impurity concentration decreasing after the second snowstorm event, when sampling 3 was collected. While the mean concentration between sampling 2 and sampling 3 decreased from 40.60 to 38.31 ng C gm^{-1}, the impurity concentrations measured during sampling 3 were expected to be more similar to sampling 1 as both of

these samplings represent freshly fallen snowpacks. One possible explanation for this outcome is the blizzard conditions during the second snow event caused significant blowing snow conditions which would locally redistribute snow and debris. Areas with increased loadings between sampling 2 and sampling 3 were primarily residential or in close proximity to tree cover as opposed to more open sites which had very low impurity concentrations measured in sampling 3. Therefore, the effects of high winds blowing snow within proximity of anthropogenic sources and tree cover should be considered. Statistical analysis of sampling 1 and sampling 3 showed that the two freshly fallen snowpacks from the Iowa filed campaign were not significantly different. This result is expected as two freshly fallen snowpacks sampled at the same site locations with similar storm trajectory origins should logically be similar.

The Big Spirit Lake sampling was designed to be the closest sampling to pure snow since it was sampled from a frozen lake that had relatively little ice fishing or snow mobile traffic, especially compared to other lakes in the area. This sampling resulted in a mean impurity concentration of 23.8 ng C gm^{-1} which was approximately equivalent to sampling 1 of the Iowa field campaign which resulted in a mean concentration of 23.05 ng C gm^{-1}. The expected result for this sampling was theorized to be lower than all other samplings; however, this finding indicates that sampling 1 of the multi-day monitoring locations was not adversely affected by local source contaminants and is more likely caused by atmospheric scavenging of impurity particles. Another result from this sampling was that a positive correlation was found between snow grain size and black carbon concentration. This agrees with the literature that as snow ages the grain size of

the snowpack increases and as grain size increased impurity concentration increased (Warren and Wiscombe, 1980).

The Belton, Texas snow sampling resulted in the highest black carbon concentration at 56.78 ng C gm^{-1}. This was 146.33% over sampling 1 and 48.21% over sampling 3 of the Iowa field campaign. The EPA emissions summary for Bell County reported that this county is in the 90^{th} percentile for dirtiest counties as a function of PM-2.5 and PM-10 emissions (Environmental Protection Agency, 2011) and has large amounts of mobile, area, and point source particulate matter emitted. Higher concentrations in this region may point to local point source emissions as the cause of increased impurity concentrations. Additionally, the longer and considerably different parcel trajectories could point to higher particulate concentrations in the atmosphere prior to scavenging during the snow event.

6.2 Sample Filter Analysis Summary

Quantification of impurities included the use of reference standard filters to provide initial loadings before later undergoing laboratory photometric analysis. A comparison of using standard reference filters versus laboratory photometric indicated that a visual acuity assessment using standard reference filters could be used in lieu of photometric analysis if necessary. A visual acuity assessment of the sample filters in comparison to the reference standards resulted in a mean impurity concentration of 40.99 ng C gm^{-1}. This result was analogous to the laboratory reported photometric results of 39.71 ng C gm^{-1}. Statistical analysis showed that there was not a statistically significant difference between a visual assessment of a set of filters to the reference standards and

photometric analysis. This indicates that comparing field samples to a set of reference standards is a feasible method for determining soot concentrations.

This is an important finding as spectrophotometer equipment is not readily available due to the expensive nature of this machinery. Research programs and institutions exploring this line of research with minimal funding could employ a visual assessment against a set of reference standards providing similar findings for a fraction of the cost of photometric analysis.

6.3 ADEOS-II/GLI Algorithm Summary

Validation of the ADEOS-II snow product algorithm that compares simulated radiances to measured sensor radiances for retrieval of snow grain size and mass fraction of soot in snow was attempted. Unfortunately, the algorithm was unable to conclusively identify a particular snow grain size and soot concentration that that would lead to a converging solution for the two spectral bands. Not only did the algorithm solution fail to uniquely identify the snow parameters, but the output snow parameter ranges did not coincide with *in situ* measurements of those properties. *In situ* measurements of snow impurities and grain size resulted in considerably lower quantification of these properties.

This result is of interest since the values measured *in situ* for these snow parameters agree with published measurements in the literature for freshly fallen snowpacks. Globally available snowpack measurements range from 1 ng C gm^{-1} to 800 ng C gm^{-1}. The MODIS validation site had an impurity concentration of 23.8 ng C gm^{-1} (0.238 ppm). This impurity measurement also falls within the values returned by the

snow products algorithm evaluated. The algorithm LUTs for snow impurities range between 0.02 and 2.5 ppmw (Stamnes et al., 2007). Additionally, snow grain size measured at the MODIS validation site ranged from 39 – 79 μm. Once again, this falls within the range of values defined in the literature for freshly fallen snow. Stamnes et al. (2007) defined that the average grain size for new snow ranges from 40 – 100 μm; while Aoki et al. (2000) used a more conservative range of 50 – 100 μm. The values considered in the LUT for snow grain size range from 40 – 1500 μm, covering the range of snow grain sizes seen in nature (Stamnes et al., 2007). With *in situ* snow parameter measurements that have resulted in values in agreement with the literature it is surprising that the algorithm grossly overestimated these properties in this particular case.

7. CONCLUSIONS

As far as the author is aware, this is the first study of its kind to evaluate the relationship between spectral albedo and mass impurities in the prairie snowpacks of the North American Great Plains. Measurements in freshly fallen prairie snowpacks in Northwestern Iowa and Central Texas were collected from February 25 to March 3, 2007 and April 6, 2007, respectively. Multi-day monitoring locations and Big Spirit Lake were use to collect snow samples to measure soot in snow concentrations.

Soot observations indicate prairie snowpack concentrations ranging from 1 ng C gm^{-1} to 115 ng C gm^{-1} with an average of 34.9 ng C gm^{-1}. Snow impurity concentrations measured in two major Great Plains snow storms are consistent with the published literature. They are higher than reported values in the Polar Regions, but lower than published measurements for China and Japan. Differences in soot concentration were observed between the two Iowa snowfall events. As expected, snow impurity concentrations were lower for freshly fallen snowpacks than aging snow as impurity concentration increased significantly over twenty-four hours following a major snow event. Furthermore, spectral albedo was found to decrease with increasing impurities. Additionally, as grain size increased impurity concentration increased. The Texas event had higher soot concentrations than both Iowa snowfalls.

The ADEOS-II\GLI snow grain size and impurity algorithm did not reproduce the measured properties from the field campaign. The algorithm was unable to uniquely identify a specific snow grain size and mass fraction of soot; in all MODIS images

processed the simulated radiances for the two spectral bands utilized in the algorithm resulted in a diverged solution. This was an unforeseen outcome as the *in situ* data at the validation site fell within published ranges for freshly fallen snow for both snow grain size and soot concentration; however; the algorithm results were considerably higher than in situ measurements.

This research on North American prairie snowpacks can be combined with published measurements to gain a better understanding of the effects and radiate forcing that black carbon has on the climate.

REFERENCES

Abramoff, M. D., Magelhaes, P. J., & Ram, S. J. (2004). Image Processing with ImageJ. *Biophotonics International*, *11*(7), 36-42.

Aoki, Te., Aoki, Ta., Fukabori, M., Hachikubo, A., Tachibana, Y., & Nishio, F. (2000). Effects of snow physical parameters on spectral albedo and bidirectional reflectance of snow surface. *Journal of Geophyical Res*earch, *105*, 10219–10236.

ASD Incorporated. (2008). Field Spec Product Specifications. *http://www.asdi.com/products-fs3.asp*, (accessed 17 January 2008).

Barkstrom, B. R. (1972). Some effects of multiple scattering on the distribution of solar radiation in snow and ice. *Journal of Glaciology*, *9*, 154–156.

Barkstrom, B. R., & Querfeld, C.W. (1975). Concerning the effect of anisotropic scattering and finite depth on the distribution of solar radiation in snow. *Journal of Glaciology*, *14*, 107–124.

Berger, R. H. (1979). Snowpack optical properties in the infrared. *CRREL Report. 79–11*, U.S. Army Cold Reg. Res. and Eng. Lab., Hanover, N. H.

Bohren, C. F., & Barkstrom, B. R. (1974). Theory of the Optical Properties of Snow. *Journal of Geophysical Research*, *79*(30), 4527–4535.

Bond, T. C., Streets, D. G., Yarber, K. F., Nelson, S. M., Woo, J. H., & Klimont, Z. (2004). A technology-based global inventory of black and organic carbon emissions from combustion. *Journal of Geophysical* Research, *109*, 14203–14246.

Choudhury, B. J., & Chang, A. T. C. (1979a). Two-stream theory of reflectance of snow. *IEEE Transactions on Geoscience Electronics, 17*(3), 63–68.

Choudhury, B. J., & Chang, A. T. C. (1979b). The solar reflectance of a snow field. *Cold Regions Science and Technology*, *1*(2), 121–128.

Choudhury, B. J., & Chang, A. T. C. (1981). On the angular variation of solar reflectance of snow. *Journal of Geophysical Research*, *86*, 465–472.

Clarke A. D. (1982a). Integrating sandwich: a new method of measurement of the light absorption coefficient for atmospheric particles. *Applied Optics*, *21*, 3011–3020.

Clarke A. D. (1982b). The effects of filter internal reflection coefficient on light absorption measurements made using the integrating plate method. *Applied Optics*, *21*, 3021–3031.

Clarke, A. D., & Noone, K. J. (1985). Soot in the Arctic snowpack: a cause for perturbations in radiative transfer. *Atmospheric Environment*, *12*, 2045–2053.

Clarke, A. D., Noone, K. J., Heintzenberg, J., Warren, S. G., & Covert, D. S. (1987). Aerosol light absorption measurement techniques: analysis and intercomparisons, *Atmospheric Environment*, *21*, 1455–1465.

Davis, R. E., Dozier, J., & Perla, R. (1987) Measurement of snow grain properties, In H.G. Jones & W.J. Orville-Thomas (Eds.), *NATO Advanced Institute on Seasonal Snowcovers: Physics, Chemistry, Hydrology* (p.63–74). Dordrecht, Holland: D. Reidel Publishing Company.

Doherty, S. J., Warren, S. G., Grenfell, T.C., Clarke, A. D., & Brandt, R. E. (2010). Light-absorbing impurities in Arctic snow. *Atmospheric Chemistry and Physics*, *10*, 11647–11680.

Draxler, R. R., & Rolph, G. D. (2003). HYSPLIT (Hybrid Single-Particle Lagrangian Integrated Trajectory) Model access via NOAA ARL READY Website. *http://www.arl.noaa.gov/HYSPLIT.php*, (accessed 2 February 2011).

Dunkle, R., Bevans, J. T. (1956). An approximate analysis of the solar reflectance and transmittance of a snow cover. *Journal of Meteorology*, *13*, 212–216.

Environmental Protection Agency. (2011). Environmental Protection Agency Reports and Maps. *http://www.epa.gov/air/data/emcatrep.html*, (accessed 7 March 2011).

Forster, P., Ramaswamy, V., Artaxo, P., Berntsen, T., Betts, R., Fahey, D. W., Haywood, D., Lean, J., Lowe, D. C., Myhre, G., Nganga, J., Prinn, R., Raga, G., Schulz, M., & Van Dorland, R. (2007). Changes in Atmospheric Constituents and in Radiative Forcing. In S. Solomon, D. Qin, M. Manning, Z. Chen, M. Marquis, K.B. Averyt, M.Tignor & H.L. Miller (Eds.), *Climate Change 2007: The Physical Science Basis. Contribution of Working Group I to the Fourth Assessment Report of the Intergovernmental Panel on Climate Change* (Chapter 2). Cambridge: Cambridge University Press.

Giddings, J. C., & Lachapelle, E. (1961). Diffusion theory applied to radiant energy distribution and albedo of snow. *Journal of Geophysical Research, 66*, 181–189.

Grenfell, T. C., Light, B., & Sturm, M. (2002). Spatial distribution and radiative effects of soot in the snow and sea ice during the SHEBA experiment. *Journal of Geophysical Research-Oceans*, *107*, 1–5.

Grenfell, T. C., Perovich, D. K., & Ogren, J. A. (1981). Spectral albedos of an alpine snowpack. *Cold Regions Science and Technology*, *4*, 121–127.

Grenfell, T. C., Warren, S. G., & Mullen, P.C. (1994). Reflection of solar-radiation by the antarctic snow surface at ultraviolet, visible, and near-infrared wavelengths. *Journal of Geophysical Research-Atmospheres, 99*, 18669–18684

Grenfell, T. C., Warren, S. G., Radinov, V. F., Makarov, V.N., Zimov, S. A. (2009). Expeditions to the Russian Arctic to survey black carbon in snow. *Transactions American Geophysical Union*, *90*, 386–387

Grenfell, T. C., Doherty, S. J., Clarke, A. D., & Warren, S. G. (2011). Light absorption from particulate impurities in snow and ice determined by spectrophotometric analysis of filters. *Applied Optics*, *50*, 2037-2049.

Hansen, J., & Nazarenko, L. (2004). Soot climate forcing via snow and ice albedos. *Proceedings of the National Academy of Sciences, 101*, 423–428.

Hansen, J., Sato, M., Ruedy, R., Nazarenko, L., Lacis, A., Schmidt, G.A., Russell, G., Aleinov, I., Bauer, M., Bauer, S., Bell, N., Cairns, B., Canuto, V., Chandler, M., Cheng, Y., Del Genio, A., Faluvegi, G., Fleming, E., Friend, A., Hall, T., Jackman, C., Kelley, M., Kiang, N., Koch, D., Lean, J., Lerner, J., Lo, K., Menon, S., Miller, R., Minnis, P., Novakov, T., Oinas, V., Perlwitz, Ja., Perlwitz, Ju., Rind, D., Romanou, A., Shindell, D., Stone, D., Sun, S., Tausnev, N., Thresher, D., Wielicki, B., Wong, T., Yao, M., & Zhang, S. (2005). Efficacy of climate forcings. *Journal of Geophysical Research*, *110*, D18104.

Hill, T. & Lewicki, P. (2007). *STATISTICS Methods and Applications*. Tulsa, OK: Statsoft.

Huang, J., Fu, Q., Zhang, W., Wang, X., Zhang, R., Ye, H., & Warren, S. G. (2011) Dust and black carbon in seasonal snow across northern China. *Bulletin of the American Meteorological Society*, *92*, 175–181.

Li, W., Stamnes, K., Chen, B., & Xiong, X. (2001). Snow grain size retrieved from near-infrared radiances at multiple wavelengths. *Geophysical Research Letters*, *28*(9), 1699–1702.

Lin, C. L., Baker, M. B., & Charlson, R. J. (1973). Absorption coefficient for atmospheric aerosols: a method for measurement. *Applied Optics*, *12*, 1356–1363.

Ogren, J. A., Charlson, R. J., & Groblicki, P. J. (1983). Determination of elemental carbon in rainwater. *Analytical Chemistry*, *55*, 1569–1572.

Stamnes, K. (1999a). Snow grain size/impurities (CTSK2b1). In *Algorithm Theoretical Basis Document*, (NASDA internal document), *27*. National Space Development Agency of Japan. Tokyo, Japan

Stamnes, K. (1999b). Cryosphere related algorithms (CTSK1). In *Algorithm Theoretical Basis Document*, (NASDA internal document), *28*. National Space Development Agency of Japan. Toyko, Japan.

Stamnes, K. (2003). Snow grain size retrieved at 1.64 μm (CTSK2b1_ch28). In *Algorithm Theoretical Basis Document*, (NASDA internal document), *4*. National Space Development Agency of Japan. Tokyo, Japan.

Stamnes, K., Li, W., Eide, H., Aoki, Te., Hori, M., & Storvold, R. (2007). ADEOS-II/GLI snow/ice products: Part I: Scientific basis. *Remote Sensing of Environment*, *111*, 258–273.

Tanikawa, T., Aoki, Te., & Nishio, F. (2001). Remote sensing of snow grain-size and impurities from Airborne Multispectral Scanner data using a snow bidirectional reflectance distribution function model. *Annals of Glaciology*, *34*, 74–80.

United States Census Bureau. (2010). United States Census 2010. *http://2010.census.gov/2010census/data/*, (accessed 14 March 2011).

Warren, S. G. (1982). Optical properties of snow. *Reviews of Geophysics, 20*, 67–89.

Warren, S. G. (1984). Impurities in snow: effects on albedo and snowmelt. *Annals of Glaciology*, *5*, 177–179.

Warren, S. G., Brandt, R. E., Grenfell, T. C., & McKay, C. P. (2002). Snowball earth: ice thickness on the tropical ocean. *Journal of Geophysical Research - Oceans*, *107*, C10, 3167.

Warren, S. G., & Clarke, A.D. (1990). Soot in the atmosphere and snow surface of Antarctica. *Journal of Geophysical Research*, *95*, 1811–1816.

Warren, S. G., & Wiscombe, W. J. (1980). A model for the spectral albedo of snow.2. snow containing atmospheric aerosols. *Journal of the Atmospheric Sciences*, *37*, 2734–2745

Warren, S. G, & Wiscombe, W. J. (1985). Dirty snow after nuclear war. *Nature*, *313*, 467–470.

Wiscombe, W. J., & Warren, S. G. (1980). A model for the spectral albedo of snow.1. pure snow. *Journal of the Atmospheric Sciences*, *37*, 2712–2733.

VITA

Name: Jennifer Nicole Morris

Address: Texas A&M University, Department of Geography
810 O&M Building, TAMU Mail Stop 3147,
College Station, Texas 77843-3147

Education: B.S., Geography, Texas A&M University, 2006
M.S., Geography, Texas A&M University, 2011

Professional Experience:

2007-2008 National Science Foundation Fellow, Advancing Geospatial Skills in Science and Social Science, GK-12 Fellowship

2006- 2007 Graduate Assistant, Office of the Dean, College of Geosciences, Texas A&M University

Selected Presentations and Posters:

Morris, J., Klein, A. 2008. Effects of snow impurities on the spectral albedo of prairie snowpacks. *Proceedings from the 53rd Annual Meeting of the Association of American Geographers*, Boston, Massachusetts.

Morris, J., Klein, A. 2007. Impurities in snow: effects on spectral albedo of prairie snowpacks. *Proceedings from the American Geophysical Union 2007 Fall Meeting*, San Francisco, California.

Morris, J., Klein, A. 2007.Impurities in snow: effects on spectral albedo of prairie snowpacks. *Proceedings from the Southwest Association of American Geographers 2007 Meeting*, Texas A&M University, College Station, Texas.